Engineering Structures 299 (2024) 117106

Contents lists available at ScienceDirect

Engineering Structures

journal homepage: www.elsevier.com/locate/engstruct

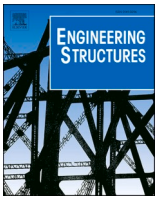

A unified approach for the prediction of the effective properties of laminated composite cellular core

Jasotharan Sriharan [a], Marcelo Dias [a], Dilum Fernando [a,*], Sondipon Adhikari [b]

[a] School of Engineering, University of Edinburgh, EH9 3FG, UK
[b] James Watt School of Engineering, The University of Glasgow, G12 8QQ, UK

ARTICLE INFO

Keywords:
Homogenisation
Strain energy
Effective properties
Laminated composite
Honeycomb core

ABSTRACT

The performance of cellular core sandwich panels is influenced significantly by the choice of geometric and material parameters of the cellular core and skins. In order to determine the optimal design of sandwich panels, it is important to relate the geometric and material parameters of the cellular core to the resulting performance of the sandwich panel. Theoretical homogenisation models are computationally efficient and plays an important role in the inverse design of sandwich panel. This paper presents a methodology to determine the equivalent homogenised properties for composite cellular core systems. The methodology was developed based on a strain energy-based homogenisation approach. Unlike other existing models, the proposed model in this paper is applicable to different core shapes and different composite wall layer configurations. An existing model was further extended for comparison purposes to determine the equivalent properties of hexagonal composite honeycomb core. Results from both models were compared with finite element (FE) results for hexagonal honeycomb cores, and the predictions from the proposed model are also compared with FE results for different cellular core shapes. A good agreement was found between the predicted and FE results. The proposed model was found to be superior to existing models in its ability to consider different core shapes and composite wall layer configurations.

1. Introduction

Sandwich structures are widely used in aerospace, automobile, civil infrastructure, and many other applications [1–9]. Sandwich structures consist of a core sandwiched between two face sheets. Key design parameters of sandwich structures, i.e. stiffness and strength depends on the mechanical and geometric properties of the core and the face sheets. Designers are given the option to select from many different materials for the face sheets, while both material and geometry choices are available for the core [10–12]. Amongst many different core types used in sandwich structures, the honeycomb core is one of the most used due to its high specific stiffness and strength [12–14]. Most of the existing honeycomb core sandwich structures have used metallic honeycomb cores, such as aluminium honeycomb and metallic or composite materials for the face sheets [15–17]. Recent developments in material and manufacturing technologies have opened the door for multi-layer composites and many different geometries to be used for cellular cores in sandwich panels [18–24]. The sandwich panels with laminated composite face sheets and cellular core are commonly referred using a term 'all-composite sandwich panels' in the literature [19]. Due to the high strength-to-weight ratio, all-composite sandwich panels are particularly attractive for applications requiring weight savings [23–24]. The versatility of the composites has revolutionized the architecture of sandwich structures by providing a variety of material and geometric choices for the core and face sheets. A large number of material and geometric choices available for sandwich cores also presents a major challenge to the designers in terms of deciding on the best material and geometry combinations for sandwich panels. For specific types of sandwich panels, including metallic or foam core sandwich panels, guidelines are available for the optimal design of the panels [25–28]. However, those guidelines cannot be directly used for composite cellular core sandwich panels due to added complexity of composite laminates (e.g., fibre direction of each lamina). So far, only limited studies have been conducted on the design optimisation of all-composite cellular core sandwich panels.

The complexity of modelling the cellular core makes the development of methodologies towards the optimal design of sandwich panels with a cellular core difficult. Generally, homogenised mechanical properties of the cellular core are used in optimising the design of the

* Corresponding author.
E-mail address: dilum.fernando@ed.ac.uk (D. Fernando).

https://doi.org/10.1016/j.engstruct.2023.117106
Received 6 June 2023; Received in revised form 1 October 2023; Accepted 29 October 2023
Available online 8 November 2023

Nomenclature

$\overline{A}_{ij}, \overline{D}_{ij}, \overline{B}_{ij}$	Membrane, bending, and membrane-bending coupling stiffness components of laminate with respect to mid-plane in $\overline{1}, \overline{2}, \overline{3}$ coordinate system
$\overline{a}_{ij}, \overline{d}_{ij}, \overline{b}_{ij}$	Membrane, bending, and membrane-bending coupling compliance components of laminate with respect to mid-plane in $\overline{1}, \overline{2}, \overline{3}$ coordinate system
$\overline{A}'_{ij}, \overline{D}'_{ij}$	Membrane and bending stiffness components of laminate with respect to the flexural neutral axis in $\overline{1}, \overline{2}, \overline{3}$ coordinate system
$\overline{a}'_{ij}, \overline{d}'_{ij}$	Membrane and bending compliance components of laminate with respect to flexural neutral axis in $\overline{1}, \overline{2}, \overline{3}$ coordinate system
ABD	Combined membrane, membrane-bending coupling, and bending stiffness matrix of laminate with respect to midplane in $\overline{1}, \overline{2}, \overline{3}$ coordinate system
b	Depth of the core
$\boldsymbol{C^H}$	Effective elasticity tensor of the core in $1, 2, 3$ coordinate system
C^H_{ijkl}	Component of the effective elasticity tensor
d	Distance between the neutral plane and mid plane of cell wall
E^H_i	Effective elastic modulus of the core
$\underline{\overline{\boldsymbol{F}}}$	Generalised nodal force vector of the wall in $\overline{1}, \overline{2}, \overline{3}$ coordinate system
$\overline{F}_{(i)j}$	Normal force at node i in the local j direction
$\overline{F}_{(i)j}$	Normal force at node i in the local j direction
G^H_{ij}	Effective shear modulus of the core
H	Compliance matrix of laminate with respect to mid plane in $\overline{1}, \overline{2}, \overline{3}$ coordinatesystem
h, l	Length of the vertical and inclined wall of the cellular core
$\overline{k}_{ij}$	Curvature of the composite wall in $\overline{1}, \overline{2}, \overline{3}$ coordinate system
$\overline{M}_{(i)}$	Moment at node i about $\overline{3}$ direction
$\boldsymbol{Q^H}$	Effective plane stress stiffness matrix of the core in $1, 2, 3$ coordinate system
Q^H_{ij}	Component of the effective plane stress stiffness matrix
$\boldsymbol{S^H}$	Effective transverse stiffness matrix of the core in $1, 2, 3$ coordinate system
S^H_{ij}	Component of the effective transverse stiffness matrix
t	Thickness of the core wall
$\boldsymbol{u}_{(i)}, \underline{\boldsymbol{u}}$	Nodal displacement vector of node i in $1, 2, 3$ and $\overline{1}, \overline{2}, \overline{3}$ coordinate systems
$u_{(i)j}, \overline{u}_{(i)j}$	Displacement of node i in the global and local j direction
$\overline{u}^a_i, \overline{u}^b_i, \overline{u}^s_i$	Normal displacement components due to axial, bending and shear in local $i$direction
ν^H_{ij}	Effective Poisson's ratio of the core
w	Strain energy density of the RVE
$\varphi(i)$	Rotation of i^{th} node about 3 direction
$\overline{\varepsilon}_{0,ij}$	Normal strain at the reference plane of composite wall in $\overline{1}, \overline{2}, \overline{3}$ coordinate system
$\overline{\varepsilon}_{ij}$	Normal strain of composite wall in $\overline{1}, \overline{2}, \overline{3}$ coordinate system
ε_{ij}	Strain component of a representative volume element of the cellular core
$\overline{\gamma}_{ij}$	Shear strain of composite wall in $\overline{1}, \overline{2}, \overline{3}$ coordinate system
$\overline{\gamma}_{0,ij}$	Normal strain at the reference plane of composite wall in $\overline{1}, \overline{2}, \overline{3}$ coordinate system
$\overline{\sigma}_{ij}$	Normal stress of composite wall in $\overline{1}, \overline{2}, \overline{3}$ coordinate system
$\overline{\tau}_{13}$	Shear stress of composite wall in $\overline{1}, \overline{2}, \overline{3}$ coordinate system

sandwich panel using failure maps or search algorithms [27–29]. Because of the inherent nature of the inverse design problem having multiple geometric and material variables, design procedure requires many iterative calculations to reach the preliminary optimal design parameters for the design. Therefore, considering computational efficiency, theoretical homogenisation models become very useful and play an important role in the inverse design of the sandwich panels.

Elastic stiffness of the sandwich panels is a key parameter affecting the performance of the sandwich panels, thus is of high importance in design of sandwich panels. Current approaches often simplify the modelling of sandwich panels by modelling the core as an equivalent shell [30–31]. Many different approaches exist towards obtaining the equivalent stiffness properties of the cellular core [32]. Amongst those, the most widely used is the force-equilibrium-based approach proposed by Gibson et al. [33]. This model assumes that honeycomb core wall response is linear-elastic and only consists of bending deformation. In calculating the bending deformation, the core wall was assumed to behave as an Euler-Bernoulli beam. Gibson et al.'s [33] model has been further refined by other researchers based on different approaches for homogenisation [34–49]. Some of these models only proposed equations to determine either in-plane or out-of-plane stiffness properties [34–45], while more advanced models considered both in-plane and out-of-plane stiffness properties [46–48]. However, most models can only predict the effective stiffness properties of the hexagonal honeycomb cores and cannot be used for other types of cellular core geometries. By adopting a strain-energy based homogenisation approach, Hohe and Becker [47–48] proposed a methodology for predicting the effective stiffness properties of cellular cores with different geometries. Some other researchers used finite element (FE) based approaches for evaluating the effective stiffness properties for different types of cellular cores [49–53]. However, FE based approaches require modelling of the representative volume elements (RVEs) of the core, thus difficult to use as a general method applicable for different types of cellular core geometries. All these methods were developed only considering isotropic cell walls for the cellular core.

When the core walls are fabricated out of multi-layered/laminated composite materials, the above models fail to predict the effective elastic properties accurately [33–49]. In multilayer composites, the effective elastic modulus measured under membrane action (called 'membrane elastic modulus' for brevity) may differ from the effective elastic modulus measured under flexural action (called 'flexural elastic modulus' for brevity) [54], which results in prediction of inaccurate effective elastic properties by the existing models. In addition, especially for asymmetric multilayer laminates, assuming the neutral plane to be the mid-plane may also not be correct, leading to inaccurate predictions of effective elastic properties by the existing models.

An analytical model for calculating the effective elastic properties of composite honeycomb core [55] was developed based on classical laminate theory (CLT) [56] and Gibson et al.'s [33] homogenisation model. Only the bending deformations of the cell walls were considered, and axial deformations were ignored. Therefore, the applicability of such model may not be accurate when axial stiffness is relatively high and/or when axial-bending coupling exists. More recently, Saether and Krishnamurthy [57] combined CLT [56] and the model given by Gibson et al. [33] to derive analytical equations to calculate the equivalent in-plane elastic properties for composite honeycomb cores. However, as

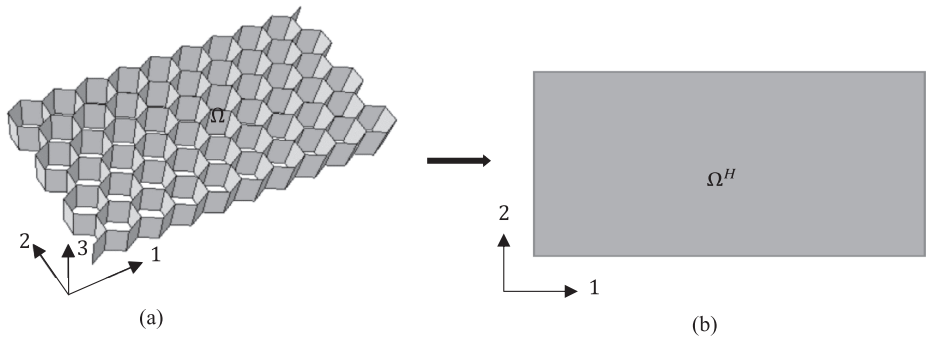

Fig. 1. Periodic cellular core structure: (a) actual configuration and (b) homogenised equivalent continuum body.

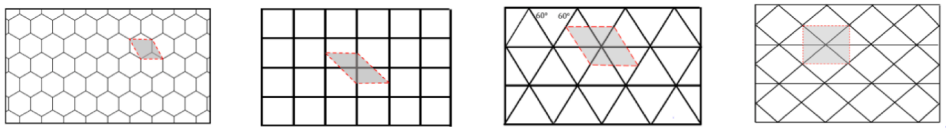

Fig. 2. RVEs of: (a) honeycomb (b) square (c) triangular and (d) mixed rhombus-triangular cellular core configuration.

only membrane elastic modulus is considered, their method fails to capture the effects due to different layer sequencing. In addition, in the example provided in Ref. [57] (Tables 12-15 in Ref. [57]), in-plane Poisson's ratio value was found to be 1. A Poisson's ratio of 1 results in infinite in-plane stiffness for the equivalent shell, thus providing inaccurate results. In addition, existing methods for composite cellular cores only considered honeycomb core; thus, the applicability of such models to other types of cellular core shapes remains unverified.

Against this background, this paper presents an investigation carried out to develop a homogenisation model for general cellular core geometries consisting of laminated composite walls. A strain energy-based approach together with CLT is used to develop a unified homogenisation model for laminated composite cellular core. Developed approach can be applied to predict the effective properties of the laminated composite cellular core with various geometric configurations. The developed method was verified against FE results of various composite cellular core configurations.

2. Proposed methodology

2.1. The general background

The ability to model a cellular core as a continuum could make modelling of the core much simpler, thus leading to models that may be used to determine the optimal design for cellular cores. Therefore, the general aim of the approach is to define an equivalent continuum model to capture the behaviour of the cellular cores with different shapes. In the proposed approach, a periodic cellular core structure (Fig. 1) with a domain Ω and an external boundary Γ is replaced with a homogenous effective continuum body Ω^H with the same shape and an external boundary Γ^H. In the strain energy-based homogenisation adopted in this study, both bodies are considered to be equivalent in terms of mechanical behaviour at the macroscopic level if the strain energy of the representative volume elements (RVEs) of both the bodies are equal under the same external loading and boundary conditions.

Condition of equivalent strain energy between the RVEs of the cellular structure and the homogenised continuum can be written as:

$$\frac{1}{V_{RVE}}\int_V w(\varepsilon_{ij})dV = \frac{1}{V_{RVE}}\int_V w^H\left(\varepsilon_{ij}^H\right)dV^H, \tag{1}$$

where $w(\varepsilon_{ij})$ and $w^H\left(\varepsilon_{ij}^H\right)$ are strain energy density of the RVEs of Ω and Ω^H respectively, V_{RVE} is the volume of the RVEs, ε_{ij} and ε_{ij}^H are strain tensor components of RVEs of the cellular core structure and the effective homogenous continuum medium respectively. Here, Latin indices, *{i, j, k, …}*, refer to the *1, 2* or *3* directions. RVEs of different types of cellular core geometries can be defined using a unit-cell parallelogram (Fig. 2), as proposed in Ref. [47].

The stiffness components C_{ijkl}^H of effective elasticity tensor for three-dimensional (3D) analysis can be derived by partial differentiation of strain energy density of the RVE with respect to strain components ε_{ij}:

$$C_{ijkl}^H = \frac{\partial^2 w}{\partial\varepsilon_{ij}\partial\varepsilon_{kl}} \tag{2}$$

Eq. (2) yields 21 independent components (C_{ijkl}^H) of effective elasticity tensor. Assuming the equivalent core at the continuum level behaves as a linear elastic orthotropic material, nine non-zero components are required to define the effective elastic stiffness tensor. In Voigt's matrix notation, the effective elastic stiffness for an equivalent orthotropic continuum core can be written as:

$$\boldsymbol{C}^H = \begin{bmatrix} C_{1111}^H & C_{1122}^H & C_{1133}^H & 0 & 0 & 0 \\ C_{1122}^H & C_{2222}^H & C_{2233}^H & 0 & 0 & 0 \\ C_{1133}^H & C_{2233}^H & C_{3333}^H & 0 & 0 & 0 \\ 0 & 0 & 0 & C_{1212}^H & 0 & 0 \\ 0 & 0 & 0 & 0 & C_{1313}^H & 0 \\ 0 & 0 & 0 & o & 0 & C_{2323}^H \end{bmatrix} \tag{3}$$

By assuming the equivalent continuum core as a shell, effective stiffness components for the equivalent shell of the core can be derived by reducing the effective elasticity matrix in Eq. (3) considering a plane-stress condition, i.e., normal stresses in direction 3 (i.e. through core thickness/outer plane direction) are zero. Plane stress effective stiffness matrix $\boldsymbol{Q}^H$ and transverse shear effective stiffness matrix $\boldsymbol{S}^H$are given as follows:

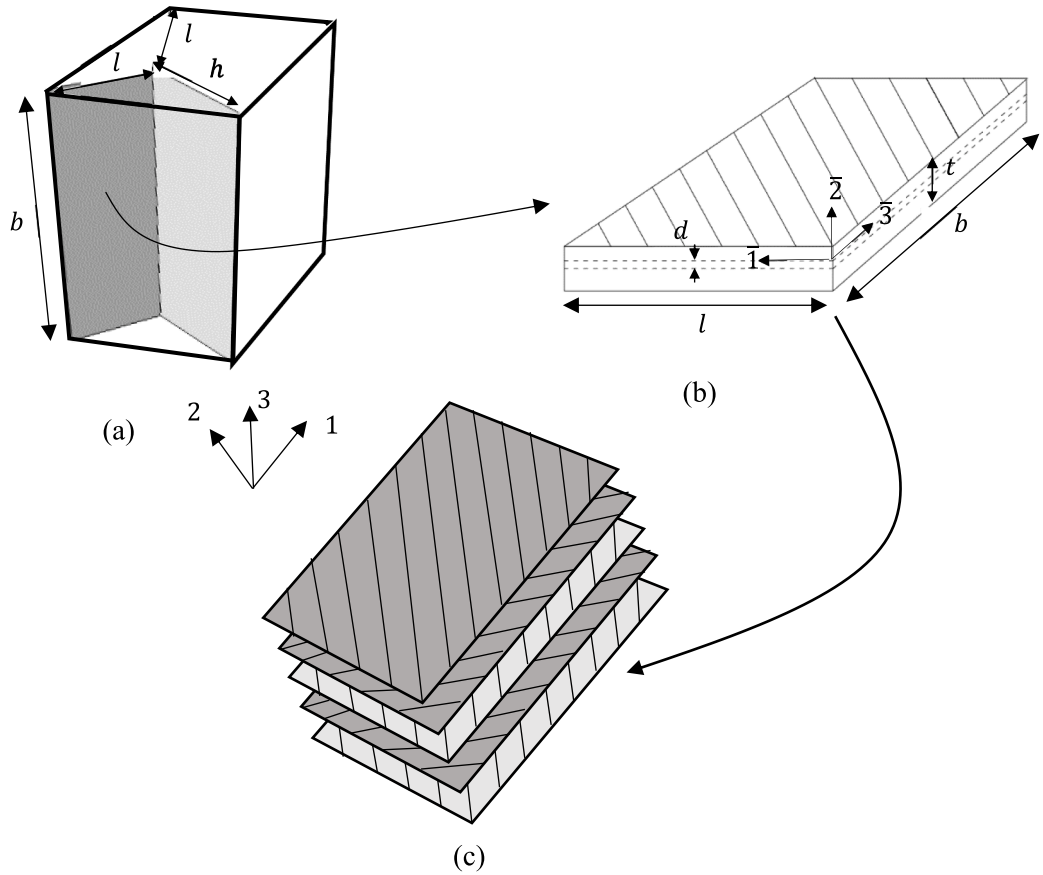

Fig. 3. (a) RVE of periodic honeycomb core fabricated out of (b) laminated composite walls consisting of (c) fibre layers at different orientations.

$$\boldsymbol{Q}^H = \begin{bmatrix} Q^H_{11} & Q^H_{12} & 0 \\ Q^H_{12} & Q^H_{22} & 0 \\ 0 & 0 & Q^H_{66} \end{bmatrix} = \begin{bmatrix} C^H_{1111} - \frac{C^H_{1133} * C^H_{1133}}{C^H_{3333}} & C^H_{1122} - \frac{C^H_{1133} * C^H_{2233}}{C^H_{3333}} & 0 \\ C^H_{1122} - \frac{C^H_{1133} * C^H_{2233}}{C^H_{3333}} & C^H_{2222} - \frac{C^H_{2233} * C^H_{2233}}{C^H_{3333}} & 0 \\ 0 & 0 & C^H_{1212} \end{bmatrix} \tag{4}$$

$$\boldsymbol{S}^H = \begin{bmatrix} S^H_{44} & 0 \\ 0 & S^H_{55} \end{bmatrix} = \begin{bmatrix} C^H_{1313} & 0 \\ 0 & C^H_{2323} \end{bmatrix}. \tag{5}$$

Effective engineering constants of the core can be calculated from the compliance matrix $\left(\boldsymbol{C}^H\right)^{-1}$, which is found from the inverse of the effective elasticity matrix:

$$\left(\boldsymbol{C}^H\right)^{-1} = \begin{bmatrix} \frac{1}{E^H_1} & -\frac{\nu^H_{21}}{E^H_2} & -\frac{\nu^H_{31}}{E^H_3} & 0 & 0 & 0 \\ -\frac{\nu^H_{12}}{E^H_1} & \frac{1}{E^H_2} & -\frac{\nu^H_{32}}{E^H_3} & 0 & 0 & 0 \\ -\frac{\nu^H_{13}}{E^H_1} & -\frac{\nu^H_{23}}{E^H_2} & \frac{1}{E^H_3} & 0 & 0 & 0 \\ 0 & 0 & 0 & \frac{1}{G^H_{12}} & 0 & 0 \\ 0 & 0 & 0 & 0 & \frac{1}{G^H_{13}} & 0 \\ 0 & 0 & 0 & 0 & 0 & \frac{1}{G^H_{23}} \end{bmatrix} \tag{6}$$

where E^H_1, E^H_2 and E^H_3 are elastic moduli in 1, 2 and 3 directions, respectively. G^H_{12} is the in-plane shear modulus, and G^H_{13} and G^H_{23} are out-of-plane shear moduli. ν^H_{12} and ν^H_{21} are in-plane Poisson's ratios, and ν^H_{13}, ν^H_{31}, ν^H_{23} and ν^H_{32} are out-of-plane Poisson's ratios. If the strain energy density of the core is known, the effective elastic constants in Eq. (6) can be calculated by partial differentiation of the strain energy with respect to respective strain components.

2.2. Strain energy density of RVE of the cellular core

This section presents the derivation of strain energy density for a RVE of the cellular core. When determining the strain energy for the RVE, it is necessary to use the stress–strain relationship of the composite core walls. Therefore, the stress–strain relationship based on CLT is first presented briefly for completeness.

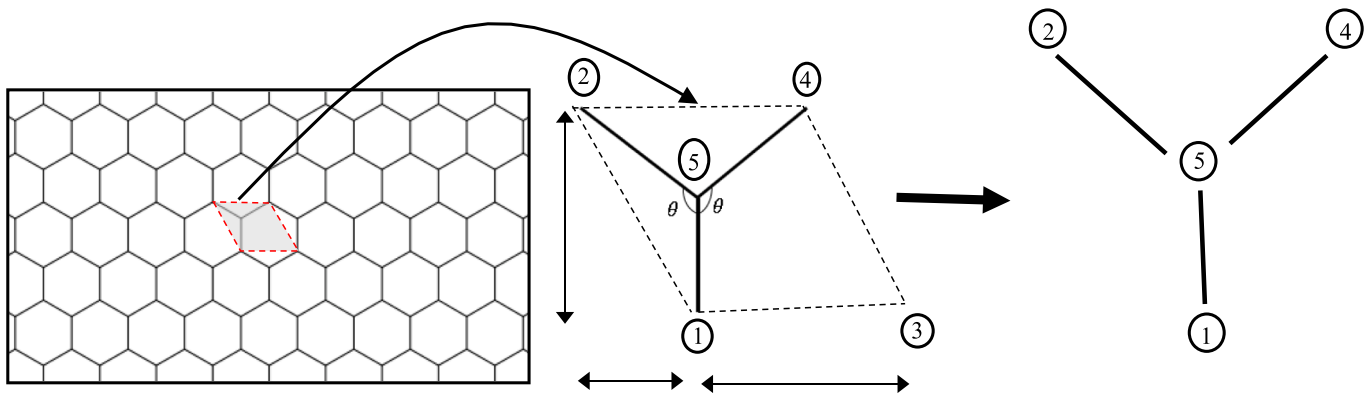

Fig. 4. The decomposition of a RVE into cell wall elements. RVE of the honeycomb core is divided into cell wall elements, and strain energy of each wall is calculated and summed up to get the strain energy of the RVE considered.

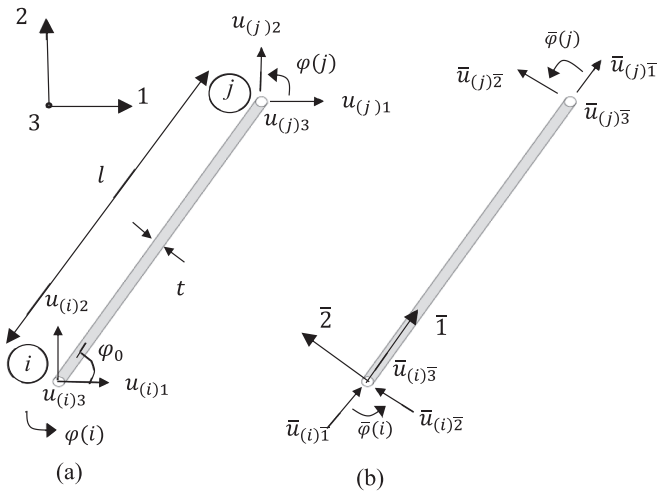

Fig. 5. Nodal displacements of the core wall in (a) global (b) local coordinates.

2.2.1. Stiffness matrix components of a composite core wall

A RVE of a periodic honeycomb core is shown in Fig. 3a, while a typical ply arrangement of a laminated composite wall of the core is shown in Fig. 3c. The combined stiffness matrix (***ABD***) and compliance matrix (***H***)of the laminated composite plate (Fig. 3b) with respect to the arbitrarily chosen reference plane[1] are respectively given by the following expressions:

$$\boldsymbol{ABD} = \begin{bmatrix} \overline{A}_{11} & \overline{A}_{13} & \overline{A}_{16} & \overline{B}_{11} & \overline{B}_{13} & \overline{B}_{16} \\ \overline{A}_{13} & \overline{A}_{33} & \overline{A}_{36} & \overline{B}_{13} & \overline{B}_{33} & \overline{B}_{36} \\ \overline{A}_{16} & \overline{A}_{36} & \overline{A}_{66} & \overline{B}_{16} & \overline{B}_{36} & \overline{B}_{66} \\ \overline{B}_{11} & \overline{B}_{13} & \overline{B}_{16} & \overline{D}_{11} & \overline{D}_{13} & \overline{D}_{16} \\ \overline{B}_{13} & \overline{B}_{33} & \overline{B}_{36} & \overline{D}_{13} & \overline{D}_{33} & \overline{D}_{36} \\ \overline{B}_{16} & \overline{B}_{36} & \overline{B}_{66} & \overline{D}_{16} & \overline{D}_{36} & \overline{D}_{66} \end{bmatrix} \tag{7}$$

$$\boldsymbol{H} = \boldsymbol{ABD}^{-1} = \begin{bmatrix} \overline{a}_{11} & \overline{a}_{13} & \overline{a}_{16} & \overline{b}_{11} & \overline{b}_{13} & \overline{b}_{16} \\ \overline{a}_{13} & \overline{a}_{33} & \overline{a}_{36} & \overline{b}_{31} & \overline{b}_{33} & \overline{b}_{36} \\ \overline{a}_{16} & \overline{a}_{36} & \overline{a}_{66} & \overline{b}_{61} & \overline{b}_{63} & \overline{b}_{66} \\ \overline{b}_{11} & \overline{b}_{31} & \overline{b}_{61} & \overline{d}_{11} & \overline{d}_{13} & \overline{d}_{16} \\ \overline{b}_{13} & \overline{b}_{33} & \overline{b}_{63} & \overline{d}_{13} & d_{33} & \overline{d}_{36} \\ \overline{b}_{16} & \overline{b}_{36} & \overline{b}_{66} & \overline{d}_{16} & \overline{d}_{36} & \overline{d}_{66} \end{bmatrix}. \tag{8}$$

If only a normal force $\overline{F}_1$ and a moment $\overline{M}_{11}$ (per unit length) are acting on the plate, axial strain ($\overline{\varepsilon}_{11}$) and curvature ($\overline{k}_{11}$) of the plane $\overline{1}-\overline{3}$ can be written as:

$$\overline{\varepsilon}_{11} = \overline{a}'_{11}\overline{F}_{11} + \overline{b}'_{11}\overline{M}_{11} \tag{9}$$

$$\overline{k}_{11} = \overline{b}'_{11}\overline{F}_{11} + \overline{d}'_{11}\overline{M}_{11}. \tag{10}$$

The components $\overline{a}'_{11}, \overline{b}'_{11}$ and $\overline{d}'_{11}$ are the elements of compliance matrix calculated with respect to the plane $\overline{1}-\overline{3}$.

To find a simple solution, in the current study, the plane $\overline{1}-\overline{3}$ is assumed to be the neutral plane for bending of the plate. In doing so, the plate is assumed to be only subjected to bending about a single axis only, and bend-twist coupling is ignored. This assumption of the neutral plane also means the coupling terms between axial and bending can be made equal to zero, i.e. $\overline{b}'_{11}$ should be equal to zero. Using the above condition, the following equation can be written for $\overline{b}'_{11}$:

$$\overline{b}'_{11} = \overline{b}_{11} + d\overline{d}_{11} = 0, \tag{11}$$

where d is the distance between the plane $\overline{1}-\overline{3}$ and the reference plane (Fig. 3b). As $\overline{b}'_{11} = 0$, d can be obtained from Eq. (11) as:

$$d = -\frac{\overline{b}_{11}}{\overline{d}_{11}}. \tag{12}$$

At the neutral plane, Eqs. (9) and (10) can be written as:

$$\overline{\varepsilon}_{11} = \overline{a}'_{11}\overline{F}_{11} \tag{13}$$

$$\overline{k}_{11} = \overline{d}'_{11}\overline{M}_{11} \tag{14}$$

Now the stiffness matrix components of the plate with respect to plane $\overline{1}-\overline{3}$ can be written as [56]:

$$\overline{A}'_{ij} = \overline{A}_{ij} \tag{15}$$

$$\overline{B}'_{ij} = \overline{B}_{ij} - d\overline{A}_{ij} = 0 \tag{16}$$

$$\overline{D}'_{ij} = \overline{D}_{ij} - 2d\overline{B}_{ij} + d^2\overline{A}_{ij}. \tag{17}$$

2.2.2. Strain energy density

The strain energy of the RVE is calculated as the sum of the strain energy of each cell wall of the RVE under applied loading and boundary conditions. A honeycomb core shown in Fig. 4 is used to demonstrate this process. An extension of the methodology to other types of periodic cellular core geometries is given at the end of this section.

The strain energy of each cell wall (Fig. 4) is calculated under plane stress conditions by solving for the nodal displacements and nodal forces

[1] In the current study, the reference plane is taken as the mid-plane of the section. The possible effects of this choice on model assumptions are discussed where necessary.

based on an assumed displacement field for the deformation of the wall. Each node of the composite core wall element consists of four degrees of freedom, i.e. translational degrees of freedom in 1, 2, and 3 directions (or $\overline{1}$, $\overline{2}$ and $\overline{3}$ directions) and rotation about axis 3 (or $\overline{3}$) (Fig. 5). In Fig. 5, $\overline{u}_{(i)1}$, $\overline{u}_{(i)2}$ and $\overline{u}_{(i)3}$ refer to the nodal displacements of the composite cell wall in the local $\overline{1}$, $\overline{2}$ and $\overline{3}$ directions respectively and $\overline{\varphi}(i)$ refers to rotation at i^{th} node about $\overline{3}$ direction. Global displacements and local displacements are related using the transformation matrix $\boldsymbol{T}$as:

$$\underline{\overline{\boldsymbol{u}}} = \boldsymbol{T}\underline{\boldsymbol{u}}, \tag{18}$$

where

$$\underline{\boldsymbol{u}} = \left\{u_{(i)1}, u_{(i)2}, u_{(i)3}, \varphi(i), u_{(j)1}, u_{(j)2}, u_{(j)3}, \varphi(j)\right\}^T, \tag{19}$$

$$\underline{\overline{\boldsymbol{u}}} = \left\{\overline{u}_{(i)1}, \overline{u}_{(i)2}, \overline{u}_{(i)3}, \overline{\varphi}(i), \overline{u}_{(j)1}, \overline{u}_{(j)2}, \overline{u}_{(j)3}, \overline{\varphi}(j)\right\}^T, \tag{20}$$

and

$$\boldsymbol{T} = \begin{bmatrix} \cos(\varphi_0) & -\sin(\varphi_0) & 0 & 0 & 0 & 0 & 0 & 0 \\ \sin(\varphi_0) & \cos(\varphi_0) & 0 & 0 & 0 & 0 & 0 & 0 \\ 0 & 0 & 1 & 0 & 0 & 0 & 0 & 0 \\ 0 & 0 & 0 & 1 & 0 & 0 & 0 & 0 \\ 0 & 0 & 0 & 0 & \cos(\varphi_0) & -\sin(\varphi_0) & 0 & 0 \\ 0 & 0 & 0 & 0 & \sin(\varphi_0) & \cos(\varphi_0) & 0 & 0 \\ 0 & 0 & 0 & 0 & 0 & 0 & 1 & 0 \\ 0 & 0 & 0 & 0 & 0 & 0 & 0 & 1 \end{bmatrix} \tag{21}$$

The displacement field of each wall is assumed to consist of three components: (a) normal deformation due to axial force in the $\overline{1}-\overline{3}$ plane (Eqs. (22)–(24)), (b) normal deformation due to bending in the $\overline{1}-\overline{2}$ plane (Eqs. (25)–(27)), and (c) normal deformation due to shear in the $\overline{1}-\overline{3}$ plane (Eqs. (32)–(34)).

In the case (a), homogeneously distributed normal deformations $\overline{u}_1^a$, $\overline{u}_2^a$ and $\overline{u}_3^a$ are due to the axial force in the $\overline{1}-\overline{3}$ plane. For the wall component given in Fig. 5, homogeneously distributed normal deformations in $\overline{1}, \overline{2}$, and $\overline{3}$ due to an axial force in the $\overline{1}-\overline{3}$ plane can be written as:

$$\overline{u}_1^a = \overline{u}_{(i)1} + \frac{\overline{u}_{(j)1} - \overline{u}_{(i)1}}{l}\overline{x}_1 \tag{22}$$

$$\overline{u}_2^a = 0 \tag{23}$$

$$\overline{u}_3^a = \overline{\varepsilon}_{33}\overline{x}_3 \tag{24}$$

The normal deformation in the direction $\overline{2}$ (as in Eq. (23)) is assumed to be negligible. However, this assumption does not have any effect on the strain energy of the RVE, as the plane stress assumption is used in calculating the strain energy of each wall.

In case (b), normal deformations $\overline{u}_1^b$, $\overline{u}_2^b$ and $\overline{u}_3^b$ are due to bending in $\overline{1}-\overline{2}$ plane (about direction-$\overline{3}$). For a wall component given in Fig. 5, homogeneously distributed normal deformations in $\overline{1}, \overline{2}$, and $\overline{3}$ due to bending in $\overline{1}-\overline{2}$ plane can be written as:

$$\overline{u}_1^b = -\left(\frac{d_{11}^{'}}{b}\left(\frac{1}{2}C_1\overline{x}_1^2 + C_2\overline{x}_1 + C_3\right)\right)\overline{x}_2 \tag{25}$$

$$\overline{u}_2^b = \frac{d_{11}^{'}}{b}\left(\frac{1}{6}C_1\overline{x}_1^3 + \frac{1}{2}C_2\overline{x}_1^2 + C_3\overline{x}_1 + C_4\right) \tag{26}$$

$$\overline{u}_3^b = 0 \tag{27}$$

where $C_1, C_2, C_3 and C_4$ are obtained by applying nodal displacement values at 1 and 2:

$$C_1 = \frac{6*b}{d_{11}^{'}*l}\left(-2\frac{\overline{u}_{(j)2} - \overline{u}_{(i)2}}{l} + \overline{\varphi}_{(i)} + \overline{\varphi}_{(j)}\right) \tag{28}$$

$$C_2 = \frac{b}{d_{11}^{'}*l}\left(6\frac{\overline{u}_{(j)2} - \overline{u}_{(i)2}}{l} - 4\overline{\varphi}_{(i)} - 2\overline{\varphi}_{(j)}\right) \tag{29}$$

$$C_3 = \frac{b}{d_{11}^{'}}\overline{\varphi}_{(i)} \tag{30}$$

$$C_4 = \frac{b}{d_{11}^{'}}\overline{u}_{(i)2} \tag{31}$$

Transverse shear deformation is assumed to be negligible, and the displacement function for the bending is derived assuming the composite wall behaves as the Euler-Bernoulli beam. The reference plane for bending of the core wall was taken as the neutral plane given by Eq. (12).

In case (c), normal deformations $\overline{u}_1^s, \overline{u}_2^s$ and $\overline{u}_3^s$ are due to shear deformation in the $\overline{1}-\overline{3}$ plane. For a wall component given in Fig. 5, homogeneously distributed normal deformations in $\overline{1}, \overline{2}$, and $\overline{3}$ due to shear deformations in $\overline{1}-\overline{3}$ plane can be written as:

$$\overline{u}_1^s = 0 \tag{32}$$

$$\overline{u}_2^s = 0 \tag{33}$$

$$\overline{u}_3^s = \overline{u}_{(i)3} + \frac{\overline{u}_{(j)3} - \overline{u}_{(i)3}}{l}\overline{x}_1. \tag{34}$$

The coordinates $\overline{x}_1, \overline{x}_2$ and $\overline{x}_2$ (Eqs. (22)–(34)) are considered in $\overline{1}, \overline{2}$ and $\overline{3}$ directions, respectively. The addition of the displacement components in each direction will give the effective displacements of the core wall in each direction.

Assuming plane stress condition for the homogenised shell, $\overline{\sigma}_{22} = 0$, stress–strain relationship of any ply in the laminated composite wall can be written as:

$$\begin{Bmatrix} \overline{\sigma}_{11} \\ \overline{\sigma}_{33} \\ \overline{\tau}_{13} \end{Bmatrix} = \begin{bmatrix} \overline{Q}_{11} & \overline{Q}_{13} & \overline{Q}_{16} \\ \overline{Q}_{13} & \overline{Q}_{33} & \overline{Q}_{36} \\ \overline{Q}_{16} & \overline{Q}_{36} & \overline{Q}_{66} \end{bmatrix} \begin{Bmatrix} \overline{\varepsilon}_{11} \\ \overline{\varepsilon}_{33} \\ \overline{\gamma}_{13} \end{Bmatrix} \tag{35}$$

where $\overline{Q}_{ij}$ are the components of the stiffness matrix of the ply of the laminated composite wall in $\overline{1}-\overline{3}$ coordinate system. Strain components in Eq. (35) can be written as:

$$\overline{\varepsilon}_{11} = \overline{\varepsilon}_{0,11} + \overline{x}_2\overline{k}_{11} \tag{36}$$

$$\overline{\varepsilon}_{33} = \overline{\varepsilon}_{0,33} + \overline{x}_2\overline{k}_{33} \tag{37}$$

$$\overline{\gamma}_{13} = \overline{\gamma}_{0,13} + \overline{x}_2\overline{k}_{13} \tag{38}$$

where $\overline{\varepsilon}_{0,11}, \overline{\varepsilon}_{0,33}$and $\overline{\gamma}_{0,13}$ are the strains in the reference plane, $\overline{k}_{11}, \overline{k}_{33}$ and $\overline{k}_{13}$ are the curvatures of the core wall, and $\overline{x}_2$ is the distance between the plane considered and the reference plane (i.e. the distance to the neutral plane). Strain $\overline{\varepsilon}_{11}$ can also be obtained by differentiating the effective displacements in $\overline{1}$ direction (i.e. Eqs. (22), (25), and (32)) with respect to $\overline{x}_1$. By comparing the components of the differential of effective displacement in $\overline{1}$ direction and Eq. (36), the following relationships can be obtained:

$$\overline{\varepsilon}_{0,11} = \frac{\overline{u}_{(j)1} - \overline{u}_{(i)1}}{l} \tag{39}$$

$$k_{11} = -\frac{d_{11}^{'}}{b}(C_1\overline{x}_1 + C_2). \tag{40}$$

Differentiating the effective displacement in $\overline{3}$ direction (i.e. Eqs. (23), (26), and (33)) with respect to $\overline{x}_3$, and comparing with Eq. (37) the following relationship can be obtained:

$$\overline{\varepsilon}_{0,33} = \overline{\varepsilon}_{33} \tag{41}$$

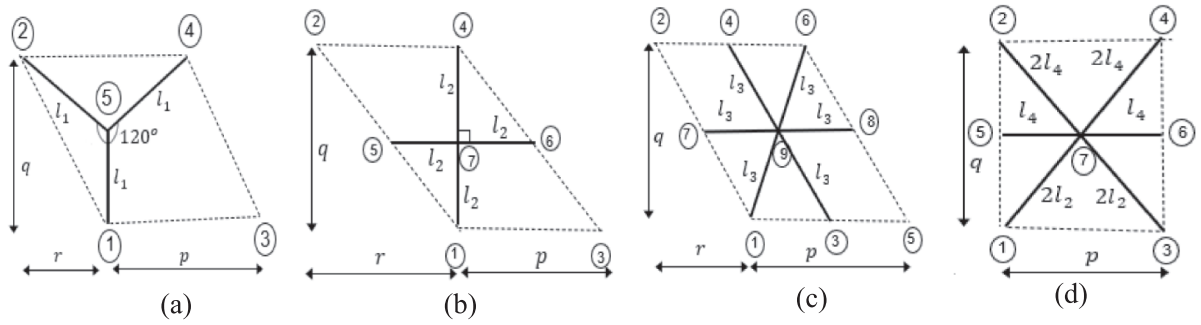

Fig. 6. RVEs of (a) honeycomb (b) square (c) triangular, and (d) mixed rhombus-triangular cellular core.

$$\overline{k}_{33} = 0 \tag{42}$$

Now, differentiating effective displacement in direction $\overline{1}$ with respect to $\overline{x}_3$ and adding that to the differential of effective displacement in direction $\overline{3}$ with respect to $\overline{x}_1$, shear strain $\overline{\gamma}_{13}$ can be obtained. Comparing that with Eq. (38), the following relationship can be established:

$$\overline{\gamma}_{0,13} = \frac{\overline{u}_{(j)3} - \overline{u}_{(i)3}}{l} \tag{43}$$

$$\overline{k}_{13} = 0 \tag{44}$$

The total strain energy of a core wall element i (i refers to core wall I, II and III in Fig. 4) can be expressed as:

$$W^i = \frac{1}{2}\int_0^l \int_0^b \int_{-(\frac{t}{2}+d)}^{(t/2-d)} (\overline{\sigma}_{11}\overline{\varepsilon}_{11} + \overline{\sigma}_{33}\overline{\varepsilon}_{33} + \overline{\tau}_{13}\overline{\gamma}_{13}) d\overline{x}_2 d\overline{x}_3 d\overline{x}_1. \tag{45}$$

By substituting Eqs. (39)-(44) into Eq. (45) and simplifying using the definition in Eqs. (15)-(17), the strain energy of the core wall element can be written as:

$$W^i = \frac{1}{2}\left(\underline{\overline{\boldsymbol{u}}}\,\overline{\boldsymbol{K}}\,\underline{\overline{\boldsymbol{u}}}^T + 2\underline{\overline{\boldsymbol{u}}}\,\overline{\boldsymbol{G}}\overline{\varepsilon}_{33} + \overline{A}_{33}\overline{\varepsilon}_{33}^2\right), \tag{46}$$

where

$$\overline{\boldsymbol{K}} = \frac{b}{l}\begin{bmatrix} \overline{A}'_{11} & 0 & \overline{A}'_{16} & 0 & -\overline{A}'_{11} & 0 & -\overline{A}'_{16} & 0 \\ 0 & \frac{12}{l^2}\overline{D}'_{11} & 0 & \frac{6}{l}\overline{D}'_{11} & 0 & -\frac{12}{l^2}\overline{D}'_{11} & 0 & \frac{6}{l}\overline{D}'_{11} \\ \overline{A}'_{16} & 0 & \overline{A}'_{66} & 0 & -\overline{A}'_{16} & 0 & -\overline{A}'_{66} & 0 \\ 0 & \frac{6}{l}\overline{D}'_{11} & 0 & 4\overline{D}'_{11} & 0 & -\frac{6}{l}\overline{D}'_{11} & 0 & 2\overline{D}'_{11} \\ -\overline{A}'_{11} & 0 & -\overline{A}'_{16} & 0 & \overline{A}'_{11} & 0 & \overline{A}'_{16} & 0 \\ 0 & -\frac{12}{l^2}\overline{D}'_{11} & 0 & -\frac{6}{l}\overline{D}'_{11} & 0 & \frac{12}{l^2}\overline{D}'_{11} & 0 & -\frac{6}{l}\overline{D}'_{11} \\ \overline{A}'_{16} & 0 & -\overline{A}'_{66} & 0 & \overline{A}'_{16} & 0 & \overline{A}'_{66} & 0 \\ 0 & \frac{6}{l}\overline{D}'_{11} & 0 & 2\overline{D}'_{11} & 0 & -\frac{6}{l}\overline{D}'_{11} & 0 & 4\overline{D}'_{11} \end{bmatrix}, \tag{47}$$

$$\overline{\boldsymbol{G}} = b\left[-\overline{A}'_{13} \quad 0 \quad -\overline{A}'_{36} \quad 0 \quad \overline{A}'_{13} \quad 0 \quad \overline{A}'_{36} \quad 0\right]^T. \tag{48}$$

Now the strain energy density of the RVE can be expressed as volume average of the sum of the strain energy of each wall in the RVE:

$$w = \frac{1}{V_{RVE}}\sum_{i=I}^{n} W^i. \tag{49}$$

2.2.3. Solving equations to get the effective stiffness components

In order to determine the strain energy of the core wall given in Eq. (46), the nodal displacement vector $\underline{\overline{\boldsymbol{u}}}$ must be known. This is possible because, first, the nodal forces are related to the nodal displacements by differentiating Eq. (46) with respect to corresponding nodal displacements. The generalised vectors of nodal forces and nodal displacements are related as given by the following expression:

$$\underline{\overline{\boldsymbol{F}}} = \overline{\boldsymbol{K}}\underline{\overline{\boldsymbol{u}}} + \overline{\boldsymbol{G}}\overline{\varepsilon}_{33}, \tag{50}$$

where

$$\underline{\overline{\boldsymbol{F}}} = \left\{\overline{F}_{(i)1} \quad \overline{F}_{(i)2} \quad \overline{F}_{(i)3} \quad \overline{M}_{(i)} \quad \overline{F}_{(j)1} \quad \overline{F}_{(j)2} \quad \overline{F}_{(j)3} \quad \overline{M}_{(j)} \right\}^T \tag{51}$$

refers to the generalized vector of nodal force of the wall element.

Using the force–displacement relationship in Eq. (50), nodal displacements of the core walls are determined considering the periodic boundary conditions. Once the nodal displacements are obtained, they can be used to determine the effective stiffness matrix components defined in Eq. (3). The procedure for obtaining effective stiffness matrix components, C^H_{ijkl} is presented in 5 steps:

Step 1: In step 1, a suitable RVE of the cellular core (e.g., as in Fig. 6) is selected.

Step 2: For the selected RVE, nine reference strain states of the RVE are selected at a time to obtain nine independent C^H_{ijkl} components of effective elasticity tensor as:

$$\begin{aligned} &\varepsilon_{ij} = \delta if : i = j, k = l \text{and} i = k \\ &\varepsilon_{ij} = \delta if : i \neq j, k \neq l, i = k \text{and} j = l \\ &\varepsilon_{ij} = \delta and \varepsilon_{kl} = \delta if : i = j, k = l \text{and} i \neq k. \end{aligned} \tag{52}$$

The volume average strain components of the RVE can be defined using Gauss's theorem as an integration around the boundary surface Γof the RVE [47,58]:

$$\varepsilon_{ij} = \frac{1}{2V_{RVE}}\int_\Gamma (u_i n_j + u_j n_i) d\Gamma, \tag{53}$$

where n_i is outward normal vector at the boundary surface Γ of the RVE.

Using Eq. (53), the average strain components of the RVE (Fig. 6a) are defined based on the characteristic dimensions and the nodal displacements of the RVE as:

$$\varepsilon_{11} = \frac{u_{(3)1} - u_{(1)1}}{p} \tag{54}$$

$$\varepsilon_{22} = \frac{u_{(2)2} - u_{(1)2}}{q} + \frac{r}{p}\frac{u_{(3)2} - u_{(1)2}}{q} \tag{55}$$

$$\varepsilon_{33} = \overline{\varepsilon}_{33} \tag{56}$$

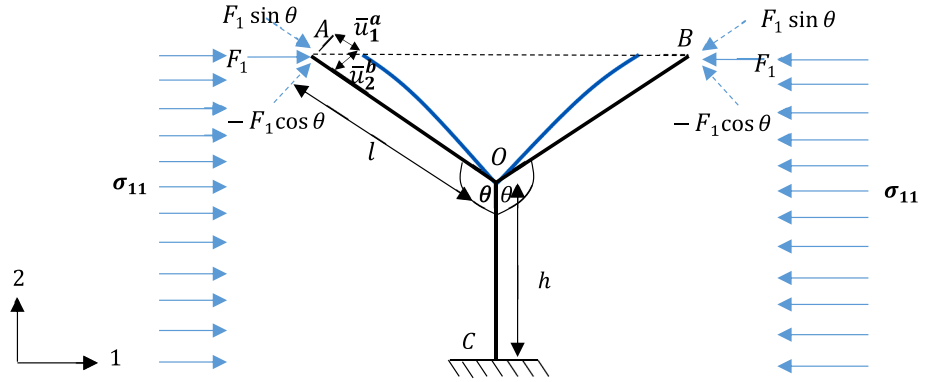

Fig. 7. Schematic diagram of deformation pattern of the unit cell under the application of uniform stress field σ_{11} in the 1-direction.

Table 1
Mechanical properties of composite wall material.

Material	$\bar{E}_1(Nmm^{-2})$	$\bar{E}_3(Nmm^{-2})$	$\bar{G}_{13}(Nmm^{-2})$	$\bar{\nu}_{13}(1)$
E-glass/Epoxy(G)	38,600	8270	4140	0.26
Boron/Epoxy(B)	204,000	18,500	5590	0.23

Table 2
Material configuration of composite wall.

Composite wall	Layer arrangement (Material properties for G and B are given in Table 1)	Fibre orientation (^{0})
1	G/G/G/G/G	45/-45/0/-45/45
2	G/G/G/G/G	0/0/90/0/0
3	G/G/G/G/G	90/0/0/0/90
4	G/G/G/G/G	0/45/90/45/0
5	G/G/G/G/G	45/0/90/0/45
6	G/G/G/G/G	45/-45/45/-45/45
7	B/G/G/G/B	45/-45/0/-45/45
8	G/B/G/B /G	0/0/90/0/0
9	B/G/G/G/B	0/0/90/0/0
10	G/B/G/B/G	90/0/0/0/90
11	G/G/B /G/G	0/45/90/45/0
12	G/G/G/G/B	45/0/90/0/45
13	B/G/G/B/G	0/0/90/0/0
14	G/G/G/G/B	45/-45/0/-45/45

$$\varepsilon_{12} = \frac{1}{2}\left(\frac{u_{(3)2} - u_{(1)2}}{p} + \frac{u_{(2)1} - u_{(1)1}}{q} + \frac{r}{p}\frac{u_{(3)1} - u_{(1)1}}{q}\right) \tag{57}$$

$$\varepsilon_{13} = \frac{1}{2}\frac{u_{(3)3} - u_{(1)3}}{p} \tag{58}$$

$$\varepsilon_{23} = \frac{1}{2}\left(\frac{u_{(2)3} - u_{(1)3}}{q} + \frac{r}{p}\frac{u_{(3)3} - u_{(1)3}}{q}\right). \tag{59}$$

Step 3: Determine the nodal displacements of each wall of the RVE with respect to local coordinates, considering the periodic boundary conditions and the equilibrium conditions of the nodal forces (see Appendix). Detailed explanations of solving for nodal displacements are not included in this paper as this has already been discussed in detail in Ref. [47].

Step 4: Calculate the strain energy of each wall (Eq. (46)) and then calculate the sum of the strain energy of all the walls in RVE and divide the total strain energy by the volume of the RVE to get the strain energy density of the RVE (Eq. (49)).

Step 5: Apply Eq. (60) to find the stiffness components of the effective elasticity tensor $\boldsymbol{C}^{\boldsymbol{H}}$:

$$C^H_{ijkl} = \begin{cases} 2w(\varepsilon_{(ij)})\dfrac{1}{\varepsilon^2_{(ij)}} if : i = j, k = landi = k \\ \dfrac{1}{2}w(\varepsilon_{(ij)})\dfrac{1}{\varepsilon^2_{(ij)}} if : i \neq j, k \neq l, i = kandj = l \\ \left(w(\varepsilon_{(ij),}\varepsilon_{(kl)}) - w(\varepsilon_{(ij)}) - w(\varepsilon_{(kl)})\right)\dfrac{1}{\varepsilon_{(ij)}\varepsilon_{(kl)}} if : i = j, k = landi \neq k. \end{cases} \tag{60}$$

The above procedure can be carried out using a simple MATLAB or Python program, thus, it can be solved for different material and cellular geometry configurations with little effort.

3. Force-equilibrium based approach

As force-equilibrium-based approach is commonly used for determining the equivalent shell properties [33–49], this section explains and employs this method for the honeycomb core. Results from this approach are compared with the previously presented strain energy-based approach. However, the applicability of the force-equilibrium approach is limited to the honeycomb core and cannot be generalised for other types of cellular core geometries, whereas the strain-energy based method is more broadly applicable.

The force-equilibrium approach considers the force-equilibrium of the walls to determine the deformation of the walls under applied uniform external stress and then the applied stress is divided by the average strain of the RVE to get the effective elastic modulus as a stress–strain ratio. Wang and Wang [55] recently proposed equations for the effective elastic properties of the composite honeycomb core. In their model, the effective in-plane Poisson's ratios for the regular hexagonal honeycomb core become equal to 1, thus resulting in singularities for Q^H_{11} and Q^H_{22}. Therefore, their model cannot be used to determine Q^H_{11} and Q^H_{22}. Mukherjee and Adhikari [37] also proposed equations to determine the effective elastic properties of the honeycomb core. Their model, together with CLT to determine composite wall properties, are used in this section to derive equations for predicting the effective in-plane properties (Q^H_{11}, Q^H_{22} and Q^H_{66}) of the composite wall honeycomb core.

The RVE of the honeycomb core, considered for calculating the effective elastic modulus in 1-direction is given in Fig. 7. A uniform stress field σ_{11} is applied to the RVE in the direction 1, as shown in Fig. 7, to derive the expression of the equivalent longitudinal elastic modulus. Applied stress field results in a force F_1 being applied at points A and B on the unit cell. The magnitude of the force F_1 is given by:

$$F_1 = \sigma_{11} b(h - l cos\theta) \tag{61}$$

Deformation $\bar{u}_2^b$ of the inclined member AO due to bending can be

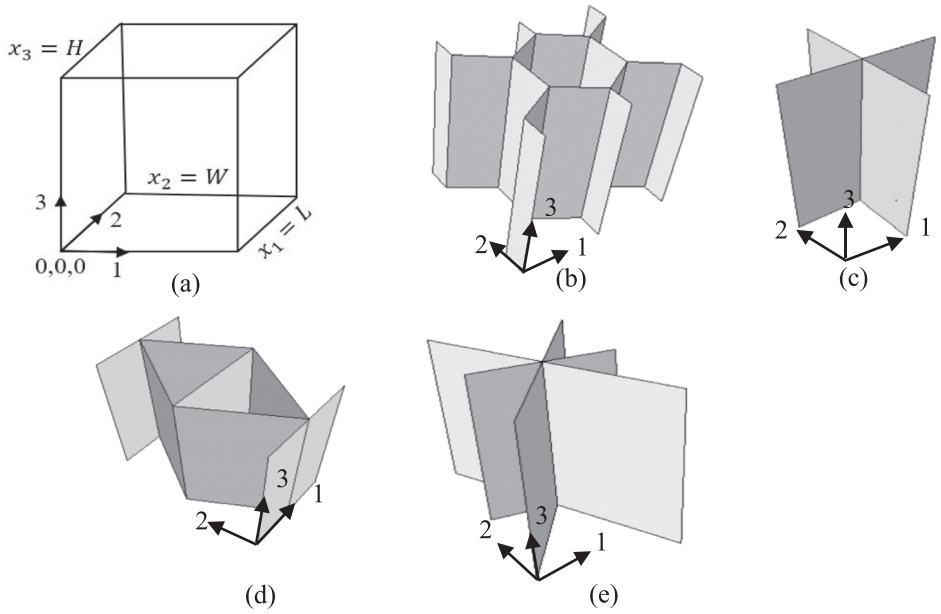

Fig. 8. (a) Boundaries of typical RVEs of (b) honeycomb (c) square (d) triangular and (e) mixed rhombus-triangular core for numerical models.

Table 3
Boundary conditions applied to RVEs to get the equivalent shell stiffness.

Effective properties	At $x_1 = 0$ $\forall x_2, x_3$	At $x_1 = L$ $\forall x_2, x_3$	At $x_2 = 0$ $\forall x_1, x_3$	At $x_2 = W$ $\forall x_1, x_3$	At $x_3 = 0$ $\forall x_1, x_2$	At $x_3 = H$ $\forall x_1, x_2$
Q_{11}^H	$u_1 = 0$All other degrees of freedom are set to free	$u_1 = 1$All other degrees of freedom are set to free	$u_2 = 0$All other degrees of freedom are set to free	$u_2 = 0$All other degrees of freedom are set to free	All degrees of freedom are set to free.	All degrees of freedom are set to free.
Q_{22}^H	$u_1 = 0$All other degrees of freedom are set to free	$u_1 = 0$All other degrees of freedom are set to free	$u_2 = 0$All other degrees of freedom are set to free	$u_2 = 1$All other degrees of freedom are set to free	All degrees of freedom are set to free.	All degrees of freedom are set to free.
Q_{12}^H	$u_1 = 0$All other degrees of freedom are set to free	$u_1 = 1$All other degrees of freedom are set to free	$u_2 = 0$All other degrees of freedom are set to free	$u_2 = 1$All other degrees of freedom are set to free	All degrees of freedom are set to free.	All degrees of freedom are set to free.
Q_{66}^H	$u_1 = u_2 = 0$All other degrees of freedom are set to free	$u_1 = 0, u_2 = 1$All other degrees of freedom are set to free	$u_1 = 0$All other degrees of freedom are set to free	$u_1 = 0$All other degrees of freedom are set to free	All degrees of freedom are set to free.	All degrees of freedom are set to free.
S_{44}^H	$u_1 = u_2 = u_3 = 0$All other degrees of freedom are set to free	$u_1 = u_2 = 0u_3 = 1$All other degrees of freedom are set to free	$u_1 = u_2 = 0$All other degrees of freedom are set to free	$u_1 = u_2 = 0$All other degrees of freedom are set to free	$u_1 = u_2 = 0$All other degrees of freedom are set to free	$u_1 = u_2 = 0$All other degrees of freedom are set to free
S_{55}^H	$u_1 = u_2 = 0$All other degrees of freedom are set to free	$u_1 = u_2 = 0$All other degrees of freedom are set to free	$u_1 = u_2 = u_3 = 0$All other degrees of freedom are set to free	$u_1 = u_2 = 0u_3 = 1$All other degrees of freedom are set to free	$u_1 = u_2 = 0$All other degrees of freedom are set to free	$u_1 = u_2 = 0$All other degrees of freedom are set to free

Table 4
Effective stiffness $\boldsymbol{Q_{11}^H}$ for the regular composite wall honeycomb core.

Composite wall	Proposed strain energy based (1) (Nmm^{-2})	Modified Mukherjee and Adhikari [37] (2)(Nmm^{-2})	FEM (3) (Nmm^{-2})	Difference $\frac{(3-1)}{3}\%$	Difference $\frac{(3-2)}{3}\%$
1	324.71	324.01	322.63	−0.64	−0.43
2	595.17	595.09	591.66	−0.59	−0.58
3	482.53	482.5	477.88	−0.97	−0.97
4	403.27	403.07	398.85	−1.11	−1.06
5	401.5	400.81	399.82	−0.42	−0.25
6	228	227.29	226.96	−0.46	−0.14
7	385.23	380.09	380.83	−1.15	0.19
8	1793.8	1793.7	1785.9	−0.44	−0.43
9	1807.1	1807	1760.7	−2.64	−2.63
10	1681.6	1681.5	1662.9	−1.12	−1.12
11	448.45	448.27	445.37	−0.69	−0.65
12	439.45	436.84	435.58	−0.89	−0.29
13	1799.7	1799.6	1715.1	−4.93	−4.93
14	360.7	357.53	356.44	−1.04	−0.3

Table 5
Effective stiffness $\boldsymbol{Q}_{22}^{\boldsymbol{H}}$ for the regular composite wall honeycomb core.

Composite wall	Proposed strain energy based (1) (Nmm^{-2})	Modified Mukherjee and Adhikari [37] (2) (Nmm^{-2})	FEM(3) (Nmm^{-2})	Difference $\frac{(3-1)}{3}\%$	Difference $\frac{(3-2)}{3}\%$
1	324.71	324.01	322.61	−0.65	−0.43
2	595.17	595.09	591.64	−0.6	−0.58
3	482.53	482.5	477.85	−0.98	−0.97
4	403.27	403.07	398.84	−1.11	−1.06
5	401.5	400.81	399.84	−0.42	−0.24
6	228	227.29	226.96	−0.46	−0.14
7	385.23	380.09	380.92	−1.13	0.22
8	1793.8	1793.7	1785.8	−0.45	−0.44
9	1807.1	1807	1760.7	−2.64	−2.63
10	1681.6	1681.5	1662.8	−1.13	−1.12
11	448.45	448.27	445.36	−0.69	−0.65
12	439.45	436.84	435.6	−0.88	2
13	1799.7	1799.6	1714.9	−4.94	−4.94
14	360.14	354.07	357.53	−1.06	−0.32

written as:

$$\overline{u}_2^b = \frac{-F_1 cos\theta}{k_{55}^l} \tag{62}$$

Deformation $\overline{u}_1^a$of the inclined wall AO due to axial forces can be written as:

$$\overline{u}_1^a = \frac{F_1 sin\theta}{k_{44}^l}. \tag{63}$$

In Eqs. (62) and (63), k_{55}^l and k_{44}^l are elements of the Euler-Bernoulli beam stiffness matrix of the inclined wall AO of length l. Considering the symmetry of elements OA and OB, the total deflection in the 1-direction can be obtained as:

$$u_1 = 2\left(\overline{u}_1^a sin\theta - \overline{u}_2^b cos\theta\right) = 2F_1\left(\frac{cos^2\theta}{k_{55}^l} + \frac{sin^2\theta}{k_{44}^l}\right)$$
$$= 2F_1\frac{cos^2\theta}{k_{55}^l}\left(1 + tan^2\theta\frac{k_{55}^l}{k_{44}^l}\right). \tag{64}$$

Hence, the strain in 1-direction is obtained as:

$$\varepsilon_{11} = \frac{u_1}{2lsin\theta} = \frac{2F_1\frac{\cos^2\theta}{k_{55}^l}\left(1 + \tan^2\theta\frac{k_{55}^l}{k_{44}^l}\right)}{2lsin\theta}. \tag{65}$$

From the normal stress and strain in direction −1, the effective elastic modulus of the honeycomb core in direction-1 can be obtained as:

$$E_1^H = \frac{\sigma_{11}}{\varepsilon_{11}} = \frac{k_{55}^l lsin\theta}{b(h - lcos\theta)\cos^2\theta\left(1 + \tan^2\theta\frac{k_{55}^l}{k_{44}^l}\right)} \tag{66}$$

If the cell walls of the honeycomb core are made of laminated composite/multi-layered material, then the stretching modulus and bending modulus of the wall could be different, and deformations must

Table 6
Effective stiffness $\boldsymbol{Q}_{12}^{\boldsymbol{H}}$ for the regular composite wall honeycomb core.

Composite wall	Proposed strain energy based (1)(Nmm^{-2})	Modified Mukherjee and Adhikari [37] (2)(Nmm^{-2})	FEM (3)(Nmm^{-2})	Difference $\frac{(3-1)}{3}\%$	Difference $\frac{(3-2)}{3}\%$
1	319.85	320.56	319.03	−0.26	−0.48
2	584.25	584.32	584.02	−0.04	−0.05
3	478.29	478.32	474.61	−0.77	−0.78
4	393.65	393.85	392.19	−0.37	−0.42
5	395.42	396.12	395.67	0.06	−0.11
6	223.19	223.9	223.49	0.14	−0.18
7	370.15	375.29	372.85	0.72	−0.66
8	1773.1	1773.2	1772.2	−0.05	−0.05
9	1759.8	1759.9	1733	−1.55	−1.56
10	1667.6	1667.7	1653.5	−0.85	−0.86
11	438.8	438.99	438.49	−0.07	−0.11
12	428.81	431.42	430.08	0.3	−0.31
13	1767.2	1767.3	1694.9	−4.26	−4.27
14	350.77	351.42	353.38	0.18	−0.56

Table 7
Effective stiffness $\boldsymbol{Q}_{66}^{\boldsymbol{H}}$ for the regular composite wall honeycomb core.

Composite wall	Proposed strain energy based(1)(Nmm^{-2})	Modified Mukherjee and Adhikari [37](2)(Nmm^{-2})	FEM (3)(Nmm^{-2})	Wang R, and Wang J. [55] (4)(Nmm^{-2})	Diff $\frac{(3-1)}{3}\%$	Diff $\frac{(3-2)}{3}\%$	Diff $\frac{(3-4)}{3}\%$
1	2.43	1.73	2.47	4.88	1.79	30.21	−97.03
2	5.46	5.38	5.37	10.97	−1.71	−0.27	−104.4
3	2.12	2.09	2.25	4.24	6.06	6.97	−88.3
4	4.81	4.61	4.75	9.68	−1.38	2.86	−103.9
5	3.04	2.34	2.93	6.1	−3.9	19.84	−108.5
6	2.4	1.69	2.39	4.83	−0.41	29.23	−101.6
7	7.54	2.4	5.7	15.15	−32.32	57.93	−166
8	10.31	10.23	9.63	20.7	−7	−6.17	−114.8
9	23.65	23.53	20.25	47.62	−16.82	−16.21	−135.2
10	6.97	6.94	6.72	13.96	−3.73	−3.32	−107.9
11	4.83	4.64	4.83	9.7	0.08	3.93	−100.9
12	5.32	2.71	3.9	9.84	−36.53	30.46	−152.4
13	16.26	16.15	14.47	32.66	−12.33	−11.6	−125.7
14	2.07	2.07	3.46	8.5	−35.25	40.12	−145.28

Table 8
Effective stiffness $\mathbf{S}_{44}^{\mathbf{H}}$ for the regular composite wall honeycomb core.

Composite wall	Proposed strain energy based (1)(Nmm^{-2})	Wang R, and Wang J. [55] (2)(Nmm^{-2})	FEM(3)(Nmm^{-2})	Difference $\frac{(3-1)}{3}$%	Difference $\frac{(3-2)}{3}$%
1	341.61	341.61	340.57	−0.31	−0.31
2	149.39	149.39	149.44	0.03	0.03
3	149.39	149.39	149.44	0.03	0.03
4	231.45	245.5	228.69	−1.21	−7.35
5	231.42	245.5	228.02	−1.49	−7.66
6	384.7	389.67	385.24	0.14	−1.15
7	745.01	961.64	735.73	−1.26	−30.71
8	170.32	170.32	169.84	−0.28	−0.28
9	170.32	170.32	170.36	0.02	0.02
10	170.32	170.32	170.36	0.02	0.02
11	243	255.97	246.76	1.52	−3.73
12	429.05	555.51	371.94	−15.36	−49.36
13	170.32	170.32	170.36	0.02	0.02
14	581.06	651.62	518.36	−12.09	−25.71

Table 9
Effective stiffness S_{55}^{H} for the regular composite wall honeycomb core.

Composite wall	Proposed strain energy based (1)(Nmm^{-2})	Wang R, and Wang J.[55] (2)(Nmm^{-2})	FEM (3)(Nmm^{-2})	Difference $\frac{(3-1)}{3}$%	Difference $\frac{(3-2)}{3}$%
1	341.61	341.61	340.57	0.06	0.06
2	149.39	149.39	149.44	0.1	0.1
3	149.39	149.39	149.44	0.1	0.1
4	231.45	245.5	228.69	−0.67	−6.35
5	231.42	245.5	228.02	−0.66	−6.35
6	384.7	389.67	385.24	0.31	−0.96
7	745.01	961.64	756.43	1.51	−21.34
8	170.32	170.32	170.41	0.05	0.05
9	170.32	170.32	170.47	0.09	0.09
10	170.32	170.32	170.47	0.09	0.09
11	243	255.97	249.05	2.43	−2.7
12	429.05	555.51	398	−7.8	−28.35
13	170.32	170.32	170.47	0.09	0.09
14	581.06	651.62	543.17	−6.97	−16.64

be calculated based on the corresponding modulus [54]. Therefore, the stiffness terms k_{55}^{l} and k_{44}^{l} in Eq. (59) and Eq. (60) should be calculated based on the equivalent elastic modulus of the wall for stretching and bending, respectively. These can be calculated and are given as follows [37]:

$$k_{44}^{l}=\left(\frac{\overline{E}_{1}^{axial}A}{l}\right)=\left(\frac{b}{l\,\overline{a}_{11}^{'}}\right) \tag{67}$$

$$k_{55}^{l}=\left(\frac{12\overline{E}_{1}^{bending}I}{l^{3}}\right)=\left(\frac{12b}{l^{3}\overline{d}_{11}^{'}}\right) \tag{68}$$

Substituting Eqs. (67) and (68) into Eq. (66), we will get the equation for the effective modulus E_1^H of laminated composite wall honeycomb core:

$$E_{1}^{H}=\frac{12sin\theta}{\left(\frac{h}{l}-cos\theta\right)\cos^{2}\theta\left(l^{3}\overline{d}_{(11),l}^{'}+12l\overline{a}_{(11),l}^{'}tan^{2}\theta\right)} \tag{69}$$

Similarly, other equations for in-plane effective elastic properties E_2^H, v_{12}^H and G_{12}^H can be derived as [37]:

$$E_{2}^{H}=\frac{k_{55}^{l}\left(\frac{h}{l}-cos\theta\right)}{b\cos^{3}\theta\left(1+cot^{2}\theta\frac{k_{55}^{l}}{k_{44}^{l}}+2\mathrm{cosec}^{2}\theta\frac{k_{55}^{l}}{k_{44}^{l}}\right)} \tag{70}$$

$$E_{2}^{H}=\frac{12\left(\frac{h}{l}-cos\theta\right)}{\sin^{3}\theta\left(l^{3}\overline{d}_{(11),l}^{'}+12l\overline{a}_{(11),l}^{'}\mathrm{cot}^{2}\theta+24h\overline{a}_{(11),h}^{'}\mathrm{cosec}^{2}\theta\right)} \tag{71}$$

$$v_{12}^{H}=-\frac{sin^{2}\theta\left(1-\frac{k_{55}^{l}}{k_{44}^{l}}\right)}{\left(\frac{h}{l}-cos\theta\right)cos\theta\left(1+tan^{2}\theta\frac{k_{55}^{l}}{k_{44}^{l}}\right)} \tag{72}$$

$$v_{12}^{H}=-\frac{sin^{2}\theta\left(l^{3}\overline{d}_{(11),l}^{'}-12l\overline{a}_{(11),l}^{'}\right)}{\left(\frac{h}{l}-cos\theta\right)cos\theta\left(l^{3}\overline{d}_{(11),l}^{'}+12l\overline{a}_{(11),l}^{'}tan^{2}\theta\right)} \tag{73}$$

$$G_{12}^{H}=\frac{\left(\frac{h}{l}-cos\theta\right)}{bsin\theta\left(-\frac{h^{2}}{2lK_{65}^{l}}+\frac{4k_{66}^{h/2}}{\left(k_{55}^{h/2}k_{66}^{h/2}-\left(k_{56}^{h/2}\right)^{2}\right)}+\frac{\left(sin\theta-\left(\frac{h}{l}-lcos\theta\right)cot\theta\right)^{2}}{k_{44}^{l}}\right)} \tag{74}$$

$$G_{12}^{H}=\frac{156\left(\frac{h}{l}-cos\theta\right)}{sin\theta\left(13h^{2}\overline{ld}_{(11),l}^{'}+2h^{3}\overline{d}_{(11),h}^{'}+156l\left(sin\theta-\left(\frac{h}{l}-lcos\theta\right)cot\theta\right)^{2}\overline{a}_{(11),l}^{'}\right)} \tag{75}$$

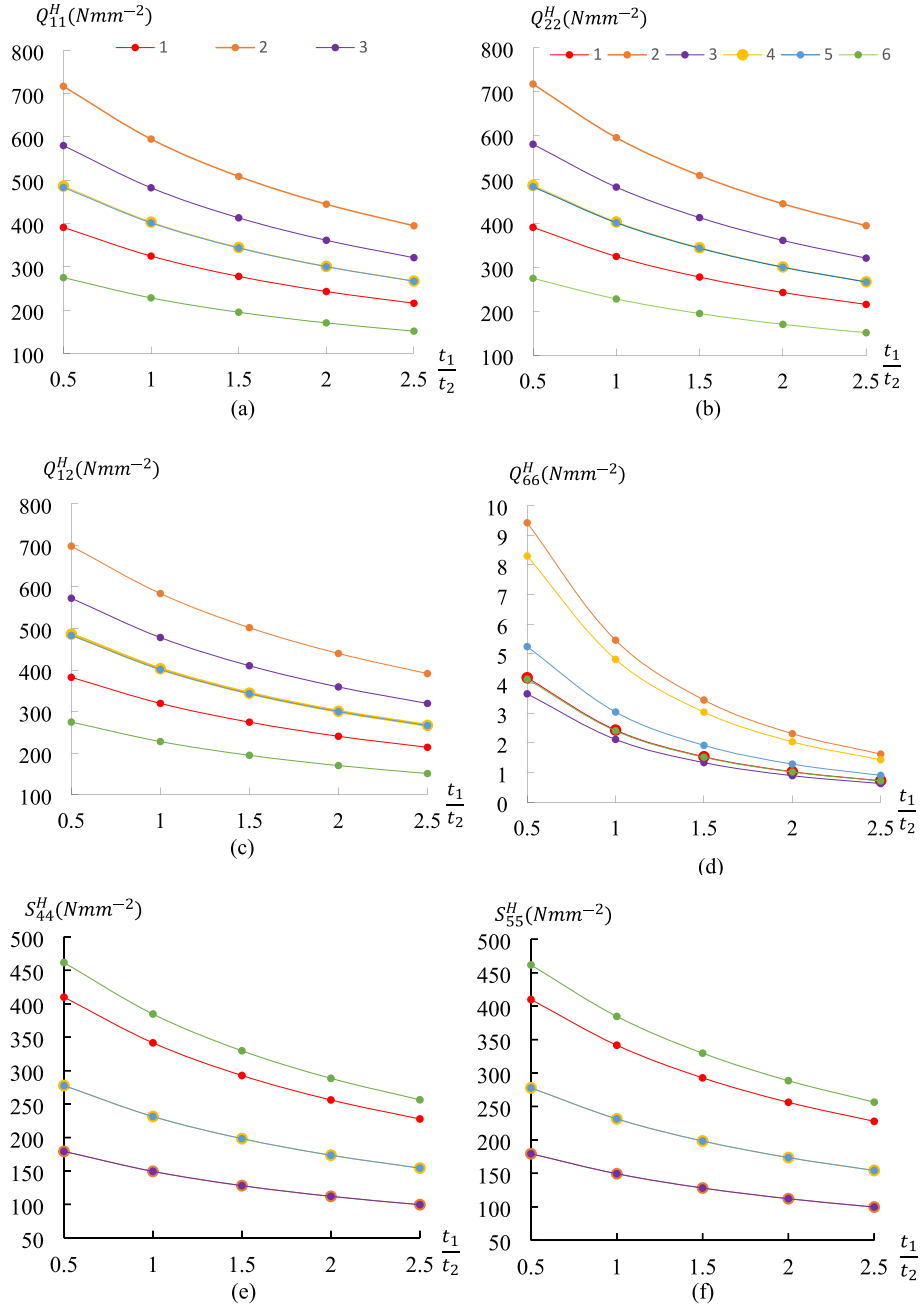

Fig. 9. Influence of vertical wall to inclined wall thickness ratio (t_1/t_2) on (a) Q_{11}^H (b) Q_{22}^H (c) Q_{12}^H (d) Q_{66}^H (e) S_{44}^H and (f) S_{55}^H of the honeycomb core.

4. Analysis of analytical derivations

To validate the proposed model, the proposed strain-energy-based model is used to calculate the effective elastic properties of an equivalent shell for RVEs of honeycomb, square, triangular, and mixed rhombus-triangular cellular core shapes (Fig. 6). Results are then compared with the equivalent shell properties obtained from FE models of the RVEs of different cellular core shapes. In addition, predictions for the honeycomb core using the proposed strain energy-based model are compared against results from the force-equilibrium based model derived based on Mukherjee and Adhikari [37], and the homogenisation model proposed by Wang and Wang [55].

Elastic properties of different FRP materials used for composite wall cellular cores with respect to principal axes of the lamina are given in Table 1. For each core shape, different composite wall layups were considered. Layer arrangements considered in this study are given in Table 2. The core wall lengths are taken as: $l_1 = l_2 = l_3 = l_4$=50 mm (Fig. 6), while the height of the cores *(b)* is taken as 150 mm. Each wall of the RVE has identical thickness and thickness of the core walls for all core shapes was selected to have a relative core density (ρ^*)of 0.0722. Each ply thickness is assumed to be equal.

RVEs of regular honeycomb, triangular, square, and mixed rhombus-triangular cellular cores (Fig. 8) were modelled using commercial software ABAQUS [59]. The S4 shell element was used with a mesh size of 10 mm selected based on a mesh convergence study. The composite shell option available in ABAQUS was used for modelling composite walls, with the material properties of each layer assigned based on properties given in Table 1, and the local material direction of each layer was assigned based on configurations given in Table 2. Prescribed displacement boundary conditions similar to [50,51] were applied according to Table 3 to get the effective properties for equivalent shell analysis. Effective properties were calculated based on the total strain

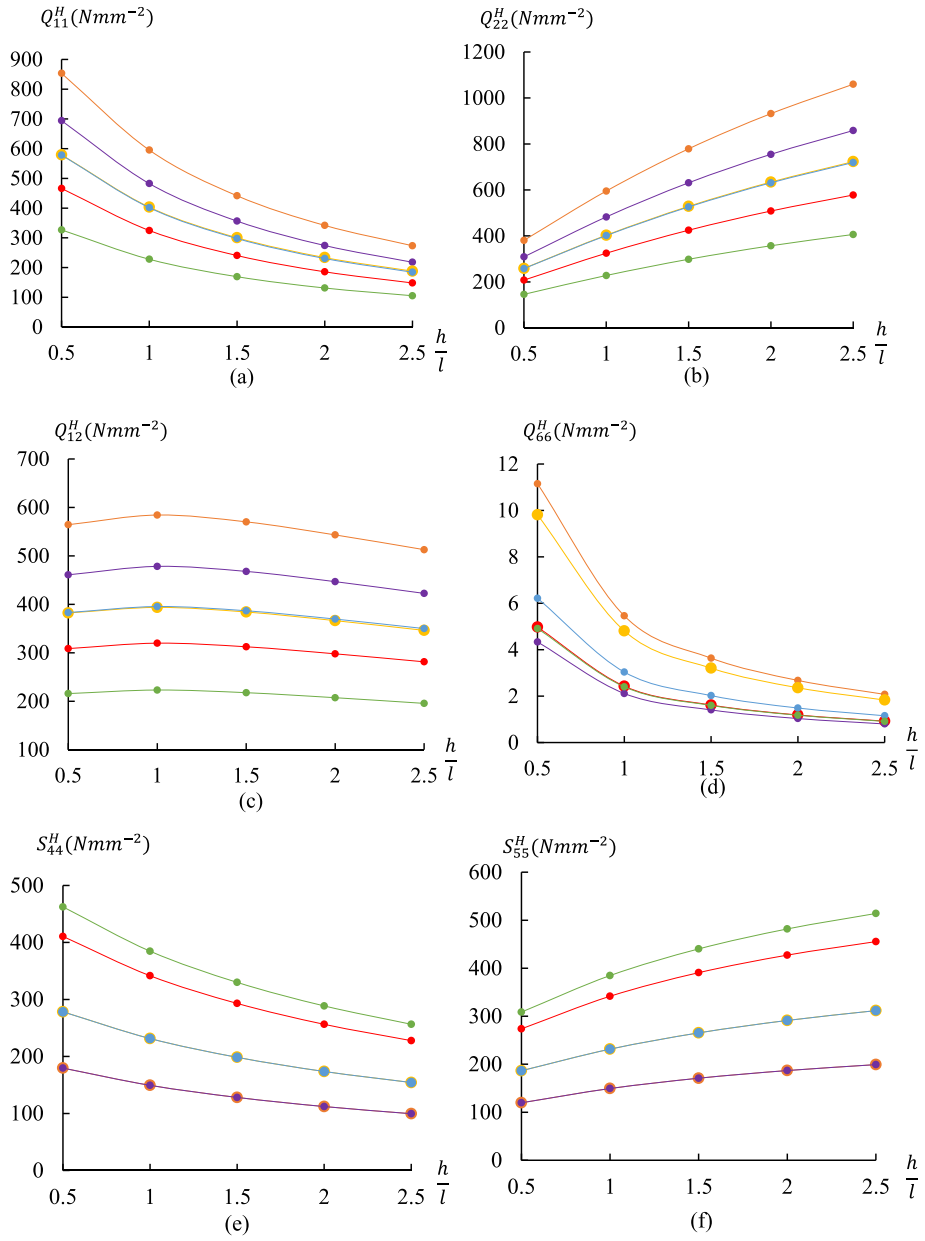

Fig. 10. Influence of vertical wall to inclined wall length ratio (h/l) on (a) $\boldsymbol{Q_{11}^H}$ (b) $\boldsymbol{Q_{22}^H}$ (c) $\boldsymbol{Q_{12}^H}$ (d) $\boldsymbol{Q_{66}^H}$ (e) $\boldsymbol{S_{44}^H}$ and (f) $\boldsymbol{S_{55}^H}$ of the honeycomb core.

energy extracted from the analysis of the RVE under applied boundary conditions.

5. Results and discussions

5.1. Hexagonal honeycomb core

Comparison of the effective in-plane properties Q_{11}^H and Q_{22}^H for the hexagonal honeycomb core RVEs predicted from the proposed strain energy-based and force-equilibrium approach (called modified Mukherjee and Adhikari [37] model hereafter) has been implemented in FE and its results are given in Tables 4 and 5. Comparison of the effective Q_{66}^H predicted from the proposed modified Mukherjee and Adhikari's and Wang and Wang's [55] models with the FE implementation are given in Table 6. In addition, effective transverse shear stiffness S_{44}^H and S_{55}^H predicted from the proposed Wang and Wang [55] model, and the FE models are also given in Tables 7 and 8.

The proposed strain-energy-based model showed an excellent agreement with the FE results, except for predictions of Q_{66}^H for several composite wall material configurations. The maximum error in predictions using the proposed model for Q_{11}^H, Q_{22}^H, Q_{12}^H and Q_{66}^H are −4.93 %, −4.94 %, −4.26 % and −36.53 % respectively (Tables 4–7). For all the properties except for Q_{66}^H, modified Mukherjee and Adhikari's model also gave good agreements with the FE results. However, predictions for Q_{66}^H from modified Mukherjee and Adhikari's model also showed a significant difference to FE results for several composite wall configurations. Wang and Wang model also showed significant differences with the FE predictions. Even for Q_{66}^H proposed strain-energy based model provided better predictions than the modified Mukherjee and Adhikari's and Wang and Wang's models. Additional comparisons for equivalent properties of the composite honeycomb core were also made with the predictions from Sather and Krishnamurthy [57] analytical models and the results are given in Sriharan [60]. The proposed model was found to provide significantly better predictions.

In predicting the transverse shear stiffness, the proposed strain energy-based model and FE results are in very good agreement for all the

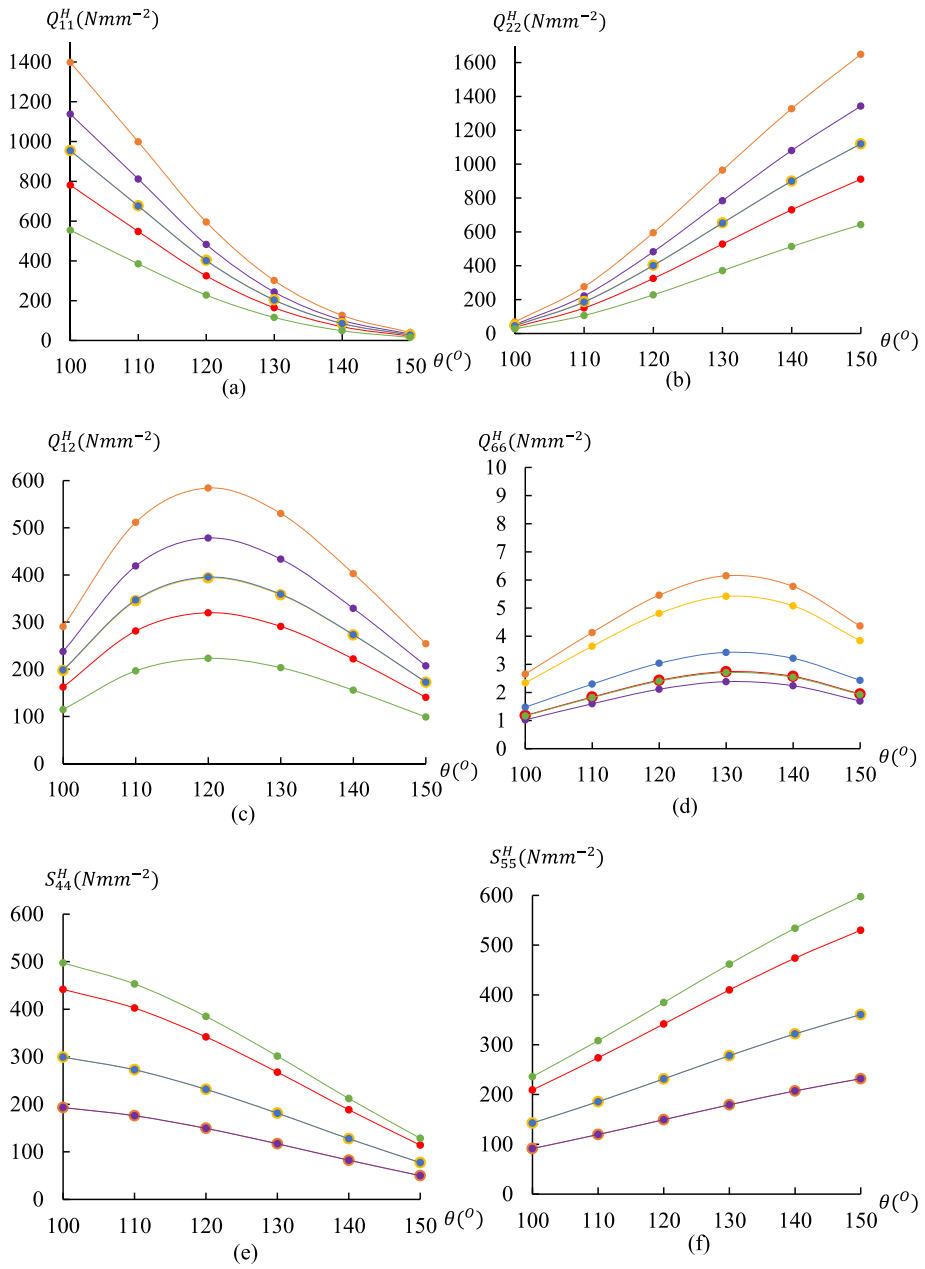

Fig. 11. Influence of angle between the vertical wall and inclined wall (θ) on (a) $\boldsymbol{Q_{11}^H}$ (b) $\boldsymbol{Q_{22}^H}$ (c) $\boldsymbol{Q_{12}^H}$ (d) $\boldsymbol{Q_{66}^H}$ (e) $\boldsymbol{S_{44}^H}$ and (f) $\boldsymbol{S_{55}^H}$ of the honeycomb core.

different material configurations of the core wall considered (Tables 8 and 9). Maximum errors in predicting S_{44}^H and S_{55}^H out of all the combinations considered are −7.8 % and −15.36 %, respectively. Wang and Wang's model predicts larger errors than the proposed model, with maximum errors of 49.36 % and −28.35 % for S_{44}^H and S_{55}^H respectively.

From the different material configurations considered, the prediction for the core consisting of symmetrically laminated walls shows excellent agreement with the FE results. The prediction accuracy reduces when the laminates are unsymmetrical and/or not orthotropic (Tables 4–9). When the laminate is not symmetrical, the membrane-bending coupling may exist. While for most cases, the condition given in Eq. (12) for considering the reference plane will eliminate this effect, for some unsymmetrical laminates, a reference plane which is also the neutral plane, may not exist within the wall thickness. In addition, when the laminate is non-orthotropic and non-isotropic, the bending-twisting coupling may also exist. As these components are not considered in the analytical models, results may deviate from the exacts when bend-twist coupling becomes stronger. However, the proposed model was shown to provide reasonable accuracy while significantly reducing the time and effort required compared to FE models in predicting effective properties for the honeycomb cores.

5.2. Parametric study

The comparisons of effective properties of the composite honeycomb core in Tables 4–9 validate the effectiveness of proposed strain energy-based model. In this section, the proposed model is used to study the influence of different variables on the effective properties of the composite honeycomb core and comparisons are shown in Figs. 9–11. In this study, core relative density (ρ^*) remains constant (0.0722) for all the cases and only material configuration 1–6 in Table 2 are considered.

Fig. 9 shows the influence of vertical wall's thickness to inclined wall's thickness ratio on the effective properties of the honeycomb core. Thickness ratio is varied keeping the length of each wall is equal to 50

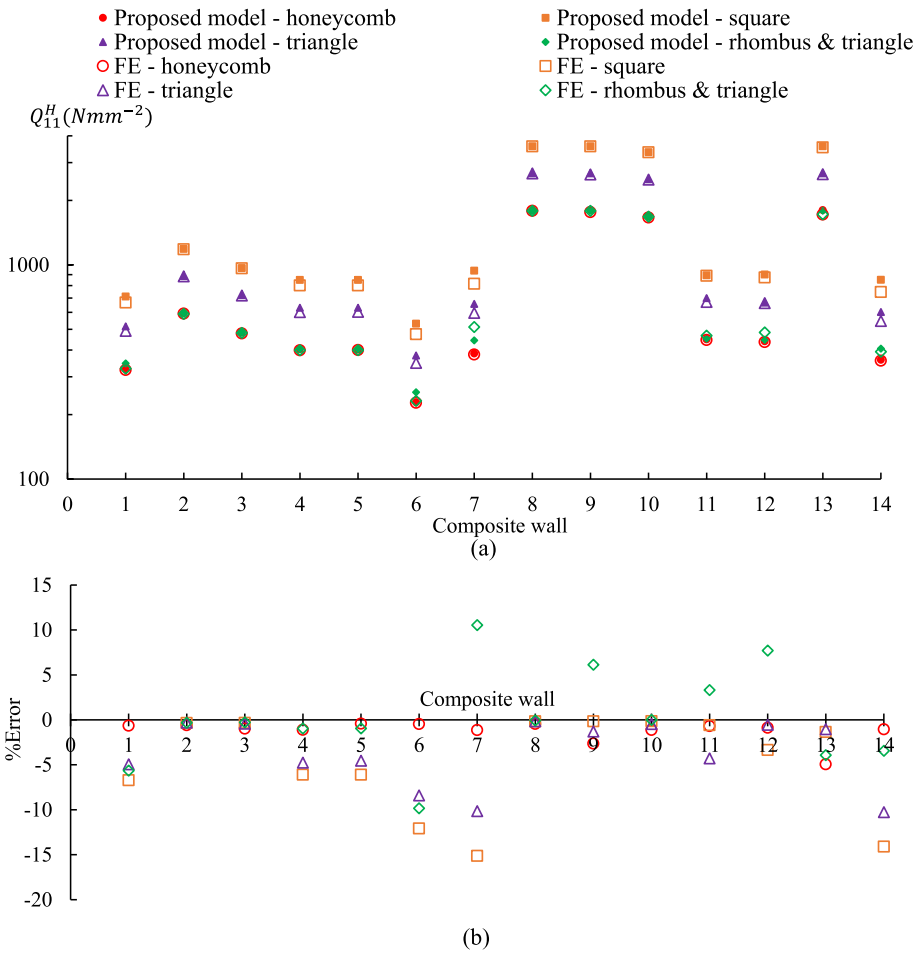

Fig. 12. Component 11 of the effective stiffness matrix (i.e., $\mathbf{Q}_{11}^{\mathbf{H}}$) for the composite wall cellular cores with different shapes and percentage error of predictions compare to FE analysis.

mm and angle between the walls is 120^0. It can be seen from Fig. 9(a)–(f) that all the effective properties decrease when the thickness ratio increases. This implies that in the regular honeycomb core, larger proportion of the loads are carried by the inclined walls and when the inclined walls get weaker, the effective stiffness of the core is reduced due to increased deformation of the inclined walls. Also, Q_{11}^H is equal to Q_{22}^H and S_{44}^H is equal to S_{55}^H means that homogenised continuum core always behaves as transversely isotropic material at the effective level regardless of the thickness ratio. Fig. 10 shows the influence of the vertical wall's length to inclined wall's length ratio on the effective properties. The length ratio between the walls is varied keeping an identical thickness (3.125 mm) for all the walls and angle between the walls is 120^0. In this case Q_{11}^H, Q_{66}^H and S_{44}^H reduce and Q_{22}^H and S_{55}^H increase when the length ratio increases. Q_{12}^H shows highest value when the ratio is 1, however it reduces continuously for further increase of length ratio (Fig. 10(a)–(f)). The reason for increase in the Q_{11}^H and S_{44}^H and reduction in Q_{22}^H and S_{55}^H can be explained by the change in average strain of the RVE caused by the change in the length ratio. The increase in the length ratio positively influences Q_{11}^H and S_{44}^H because characteristics length of RVE is decreased in direction-1 which eventually results lower average strain of core compared to direction-2. Fig. 11 shows the influence of the angle between vertical and inclined walls on the effective properties. In this case Q_{11}^H, and S_{44}^H reduce and Q_{22}^H and S_{55}^H increase with the increase of angle between the walls. Q_{12}^H shows highest value when the angle is 120^0 whereas Q_{66}^H reaches the highest value when the angle is around 130^0. Variation of different parameters positively and negatively influences the effective properties. The effect of the variation of parameters in Figs. 9–11 mainly depends on the overall geometry change of the RVE as well as the change in proportion of the loads carried by each wall due to change in geometry of individual wall.

5.3. Cellular cores with different shapes

Figs. 12–17 compares the effective properties of different cellular core shapes under the same core density, and different material configurations of the composite wall predicted using the proposed strain energy-based model and the FE analysis. The material configurations 1–14 listed in Table 2 were considered. Predicted values are plotted in Figs. 12–17.

For most of the core shapes, predictions from the proposed model agreed well with the FE results. However, predictions for Q_{12}^H and Q_{66}^H from the proposed model showed differences with the FE results for square core shape (Figs. 14 and 15). However, it was also observed that actual values of the Q_{12}^H and Q_{66}^H for square cores are relatively small. Therefore, the overall error caused by this mismatch can be expected to be small. When stiffness values are relatively large, the proposed model predictions agreed well with the FE results.

It can be seen from Figs. 12–17 that, although the core density is the same, the effective properties are different for different core shapes and material configurations. Out of all the different cellular core shapes, the square core shows the highest in-plane normal stiffness Q_{11}^H and Q_{11}^H while having the lowest in-plane shear modulus Q_{66}^H for all different material configuration considered. Moreover, it gives a very small negative Poisons' ratio resulting in the negative stiffness value for Q_{12}^H

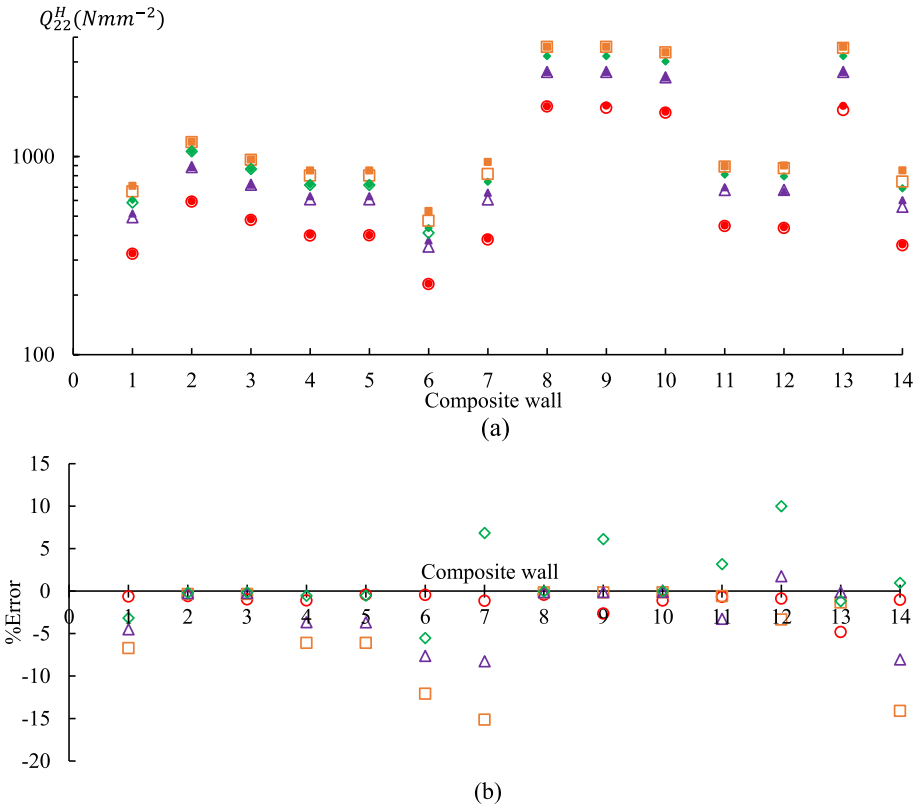

Fig. 13. Component 22 of the effective stiffness matrix (i.e., $\mathbf{Q}_{22}^{\mathbf{H}}$) for the composite wall cellular cores with different shapes and percentage error of predictions compare to FE analysis.

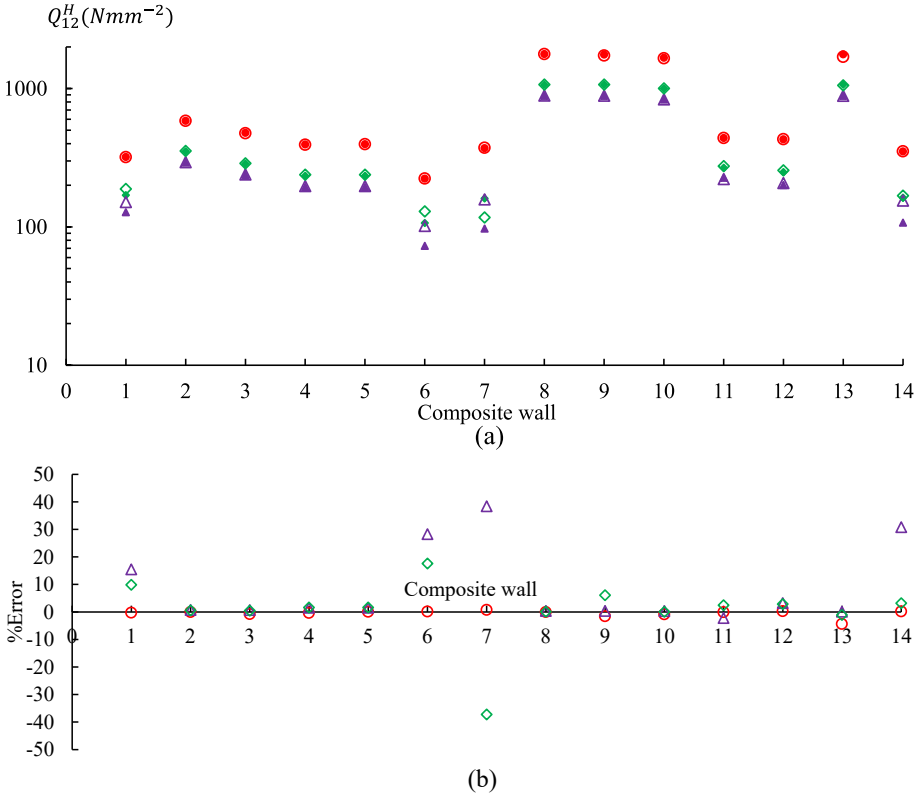

Fig. 14. Component 12 of the effective stiffness matrix (i.e., $\boldsymbol{Q}_{12}^{\boldsymbol{H}}$) for the composite wall cellular cores with different shapes and percentage error of predictions compare to FE analysis.

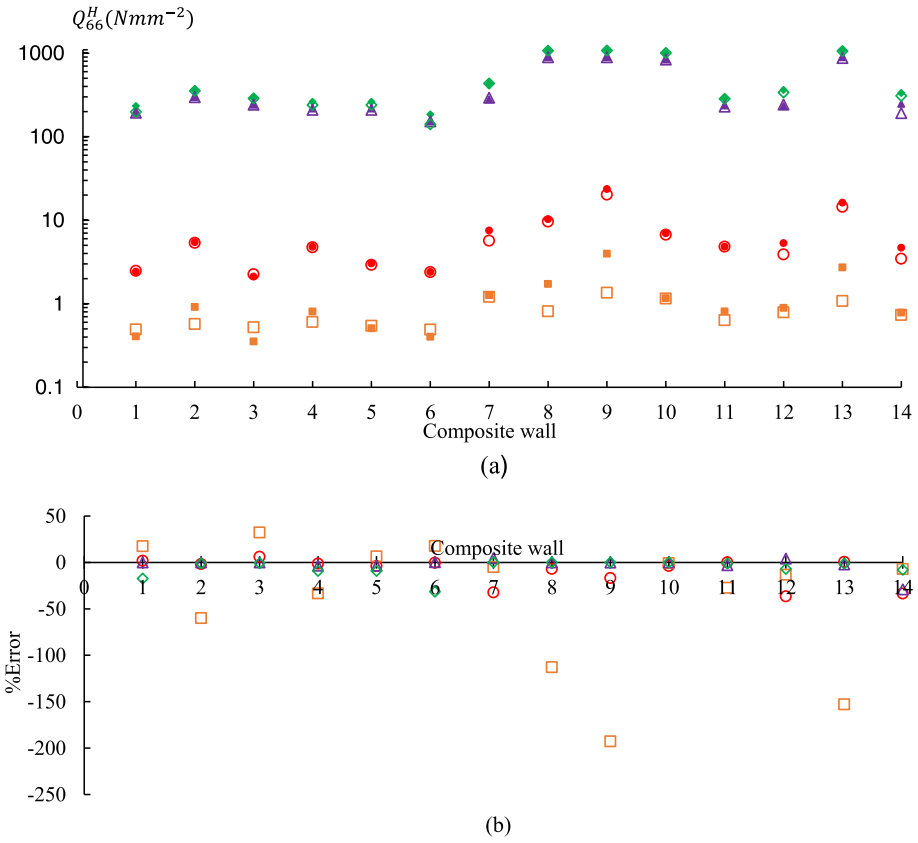

Fig. 15. Component 66 of the effective stiffness matrix (i.e., Q_{66}^{H}) for the composite wall cellular cores with different shapes and percentage error of predictions compare to FE analysis.

(Fig. 14). While the hexagonal honeycomb core shows the lowest in-plane normal stiffness, it shows the highest in-plane normal coupling stiffness Q_{12}^{H} for all the cases (Fig. 14) due to effective in-plane Poisson's ratio. The triangular core shows the highest in-plane shear stiffness out of all the core shapes considered (Fig. 15). Except for the mixed rhombus-triangular core, all the other cores behave as transversely isotropic material at the effective level, whereas mixed rhombus-triangular shows orthotropic material behaviour.

In the case of out-of-plane shear stiffness (Figs. 16 and 17), triangular, square, and honeycomb cores results in almost the same values for all the different material configurations. However, mixed rhombus-triangular core results in slightly higher values for S_{44}^{H} and lower values for S_{55}^{H} than the other core shapes. Regardless of the shapes of the cellular cores, the highest value for transverse shear stiffness was observed when the fibre layer arrangement is (45/-45), and stiffness was found to reduce when the fibre layer arrangement is (0/90) (Figs. 16 and 17).

While above-developed equations were shown to be accurate in determining the equivalent effective stiffness properties of the composite wall cellular cores, calculations are tedious and thus may not be attractive for design purposes. Therefore, simplified design plots are produced in Figs. 18–21 for calculating the effective properties of the cellular cores of different shapes. The following example demonstrated the use of design plots for obtaining the effective stiffness properties for a honeycomb core:

Example: Consider the composite wall configuration 1 and 7 in Table 2 for the hexagonal honeycomb core. For configuration 1 in Table 2, the value of the ratio $\overline{A}_{12}^{'2}/(\overline{A}_{11}^{'}\overline{A}_{22}^{'})$ is 0.17, while value of the ratio $\overline{D}_{11}^{'}/(\overline{A}_{11}^{'}l^2)$ is 2.62×10^{-4}. Using the above two values in Fig. 18 (a)–(c), values of the ratios $(Q_{11}^{H}l)/\overline{A}_{11}^{'}$, $(Q_{12}^{H}l)/\overline{A}_{11}^{'}$, and $(Q_{66}^{H}l)/\overline{A}_{11}^{'}$ can be obtained as approximately 0.2405, 0.2377, and 0.0018 respectively. Since value of the $\overline{A}_{11}^{'}$ is 6.7281×10^{4} Nmm^{-1}, the effective properties Q_{11}^{H}, Q_{12}^{H}, and Q_{66}^{H} can be calculated as 323.6 Nmm^{-2}, 319.9 Nmm^{-2}, and 2.42 Nmm^{-2} respectively.

For configuration 7 in Table 2, the value of the ratio $\overline{A}_{12}^{'2}/(\overline{A}_{11}^{'}\overline{A}_{22}^{'})$ is 0.457, while value of the ratio $\overline{D}_{11}^{'}/(\overline{A}_{11}^{'}l^2)$ is $4.35*10^{-4}$. Using the above two values in Fig. 18(a) - (c), values of the ratios $(Q_{11}^{H}l)/\overline{A}_{11}^{'}$, $(Q_{12}^{H}l)/\overline{A}_{11}^{'}$, and $(Q_{66}^{H}l)/\overline{A}_{11}^{'}$ can be obtained as approximately 0.159, 0.152, and 0.003 respectively. Since value of the $\overline{A}_{11}^{'}$ is 1.2521×10^{5} Nmm^{-1}, effective properties Q_{11}^{H}, Q_{12}^{H}, and Q_{66}^{H} can be calculated as 398 Nmm^{-2}, 380 Nmm^{-2}, and 7.5 Nmm^{-2} respectively.

Similarly, Plots 19, 20, and 21 can be used for calculating the effective properties of square, triangular, and mixed rhombus honeycomb core shapes, respectively.

6. Conclusions

This paper presented a methodology to determine the equivalent stiffness properties for a continuum-based homogenised composite cellular core, therefore providing a pathway for the designers to make better decisions on key design parameters such as cellular core shape, cell geometry, and cell wall materials and layer sequences when designing cellular core sandwich panels to meet a desired performance. Equivalent stiffness properties were determined by equating the strain energy of a representative volume element of the cellular core to the strain energy of an equivalent homogenised shell under the same resulting deformation for a given force.

The proposed methodology provides a significant advancement in the design of cellular core sandwich panel technologies by allowing

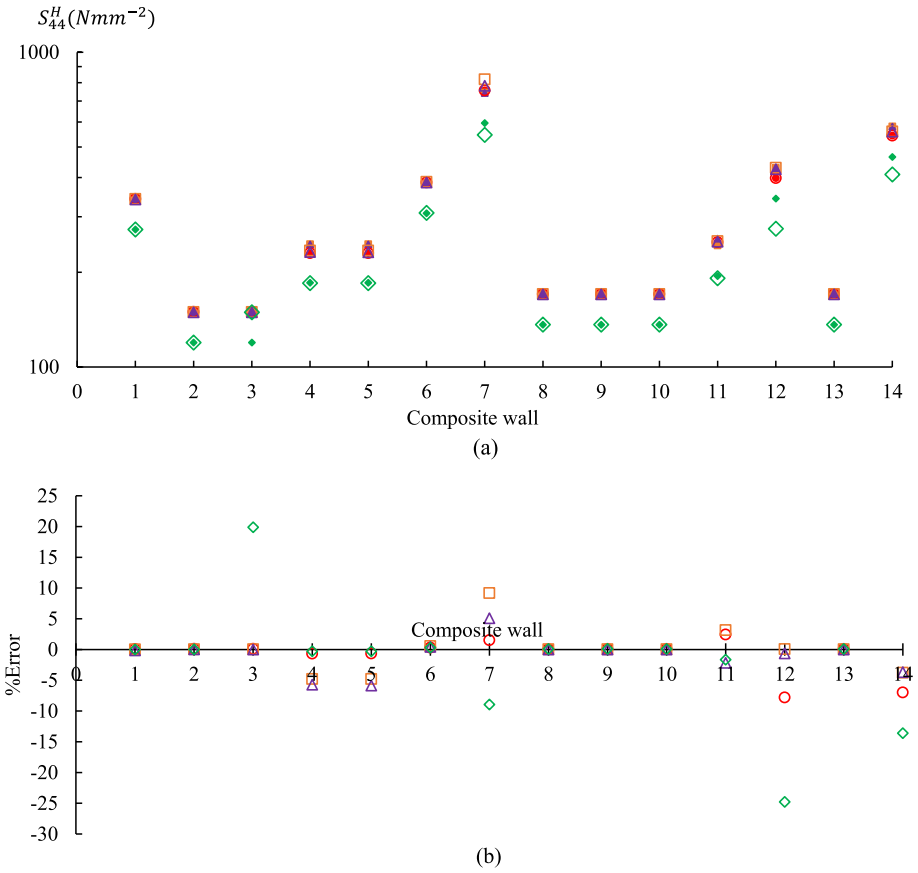

Fig. 16. Component 44 of the effective stiffness matrix (i.e., S_{44}^{H}) for the composite wall cellular cores with different shapes and percentage error of predictions compare to FE analysis.

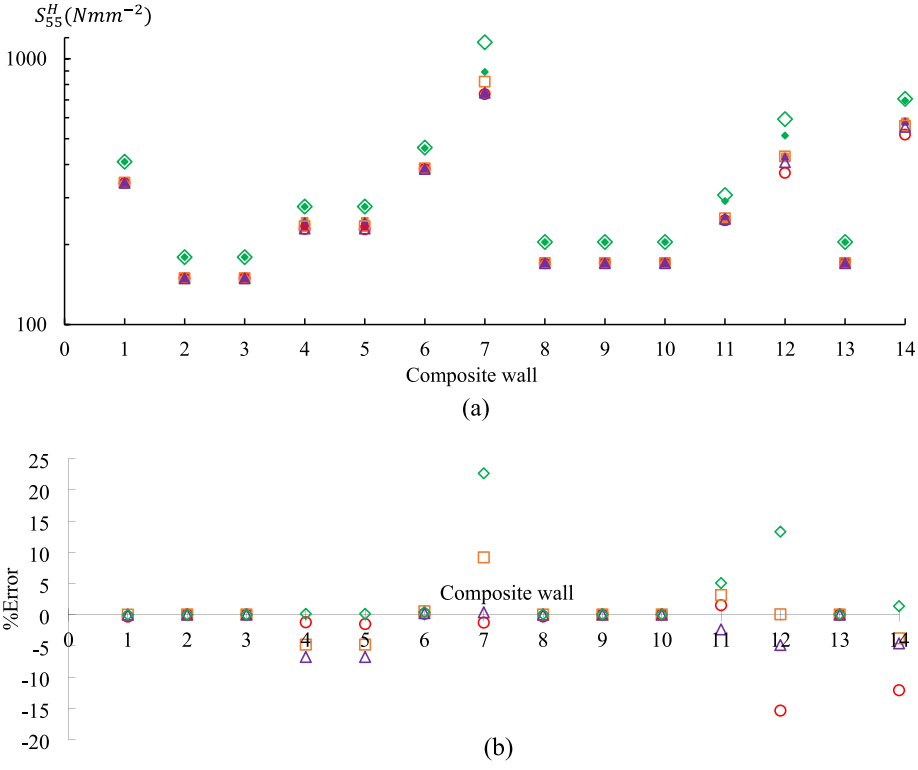

Fig. 17. Component 55 of the effective stiffness matrix (i.e., S_{55}^{H}) for the composite wall cellular cores with different shapes and percentage error of predictions compare to FE analysis.

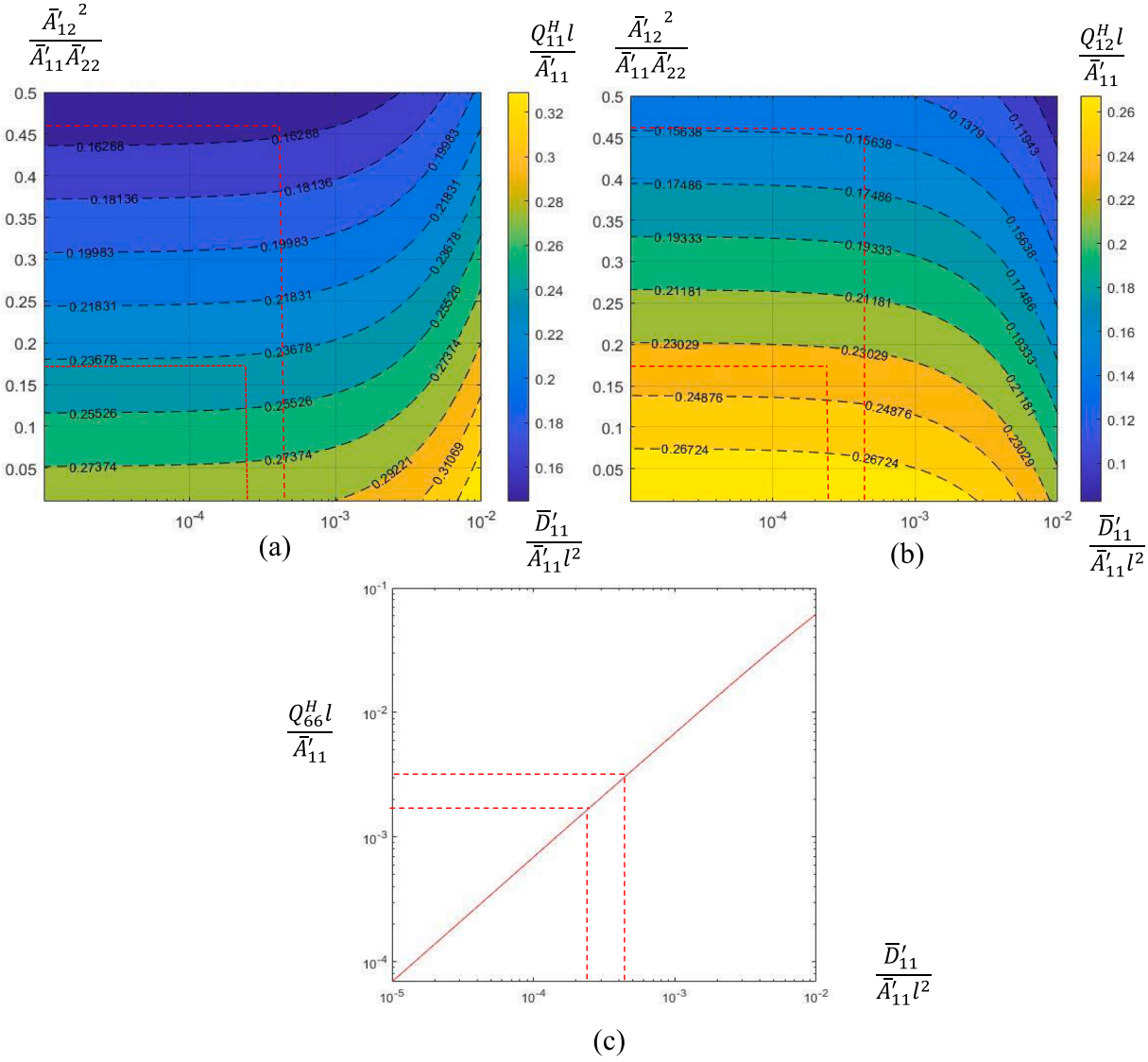

Fig. 18. Influence of wall stiffness parameters on (a) Q_{11}^H or Q_{22}^H (b) Q_{12}^H and (c) Q_{66}^H of honeycomb core.

designers to consider key design parameters such as core shape, geometry, materials, and composite layer sequences and their interactions in determining optimal designs for the required performance. The proposed methodology, breakaway the limitations in existing methodologies in terms of core shapes, materials and cell wall composite layer sequences and provide a unified approach to consider all the above in a single modelling approach.

To compare with existing methodologies for determining equivalent properties of honeycomb core, an existing model developed based on a force-equilibrium approach for the honeycomb core with isotropic materials was also extended to determine equivalent properties for composite honeycomb core (called modified-existing model). Predictions from the proposed model, a modified-existing model, and an existing model were compared with finite element (FE) results of honeycomb core with different cell wall composite layer sequences. Predictions from the proposed model were also compared with FE results for different cellular core shapes and cell wall composite layer sequences.

Comparisons showed that the proposed model provides accurate predictions for the equivalent properties of composite honeycomb core for different composite wall layer sequences. Modified-existing model also gave good predictions for the honeycomb core. Both models performed better than the other existing models. The proposed model also provided accurate predictions for different cellular core shapes. The proposed model, therefore, is superior to any other existing model in terms of its general applicability.

Simplified design plots were produced using the proposed model to calculate the effective properties of the cellular cores of different shapes. These plots are valuable in assisting the designers in determining the effective properties without having to go through a rigorous calculation process.

The proposed methodology is an important step towards the optimal design of sandwich panels. Such optimal designs will have a significant impact in many industries, such as aerospace, automobile, and civil infrastructure, in terms of efficient designs capable of reducing weight, cost, and embodied energy while meeting the intended performance requirements. To get the best benefits of this methodology, further work is required to (a) extend this methodology also to consider the skins of the sandwich panel, (b) extend this methodology to consider potential failure modes, and (c) develop optimization methods to determine the optimal sandwich panel designs.

CRediT authorship contribution statement

Jasotharan Sriharan: Investigation, Methodology, Writing –

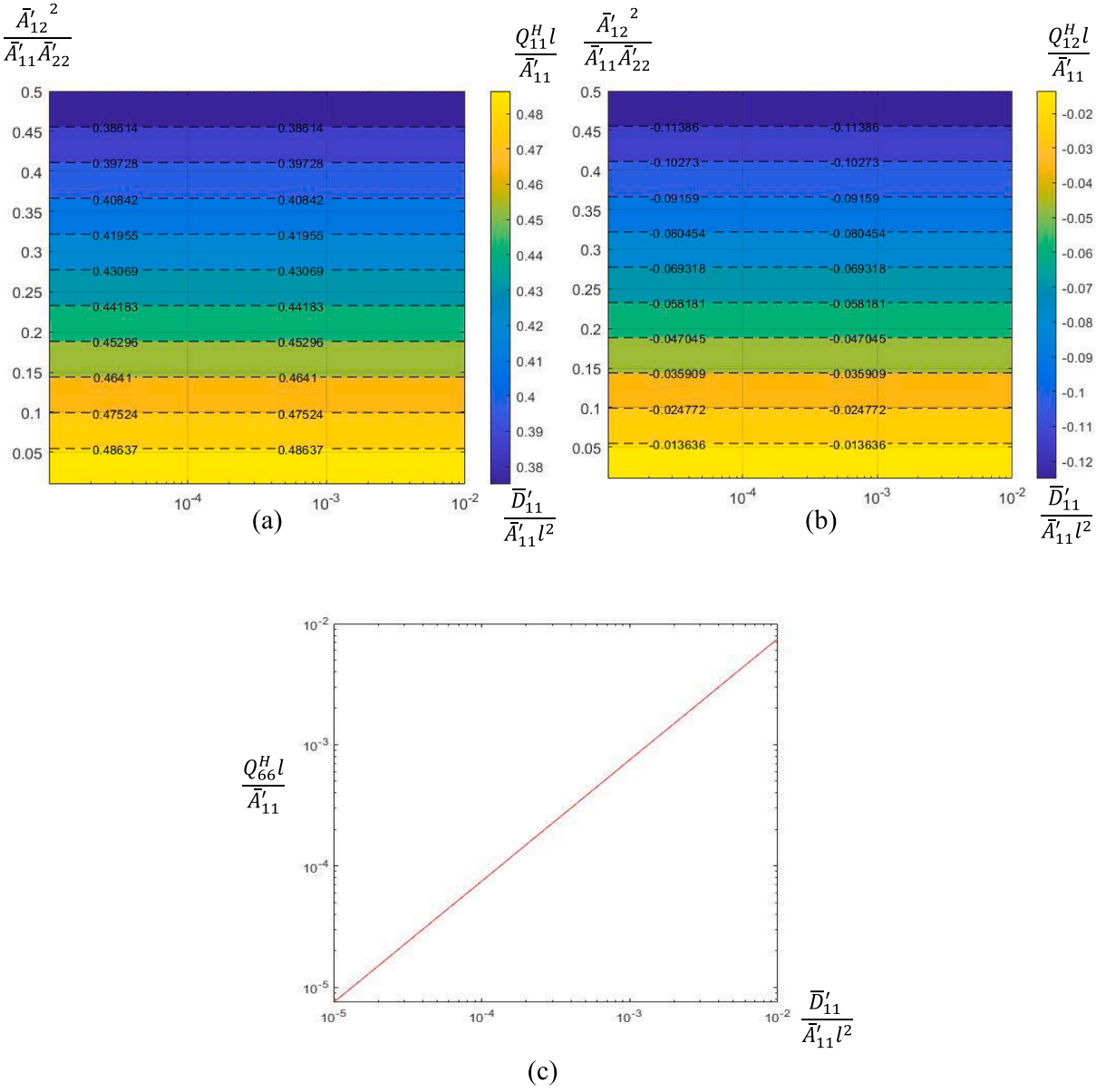

Fig. 19. Influence of wall stiffness parameters on (a) Q^H_{11}orQ^H_{22} (b) Q^H_{12} and (c) Q^H_{66} of square core.

original draft. **Marcelo Dias:** Investigation, Supervision, Writing – review & editing. **Dilum Fernando:** Investigation, Supervision, Writing – review & editing. **Sondipon Adhikari:** Investigation, Supervision, Writing – review & editing.

Declaration of Competing Interest

The authors declare that they have no known competing financial interests or personal relationships that could have appeared to influence the work reported in this paper.

Data availability

Data will be made available on request.

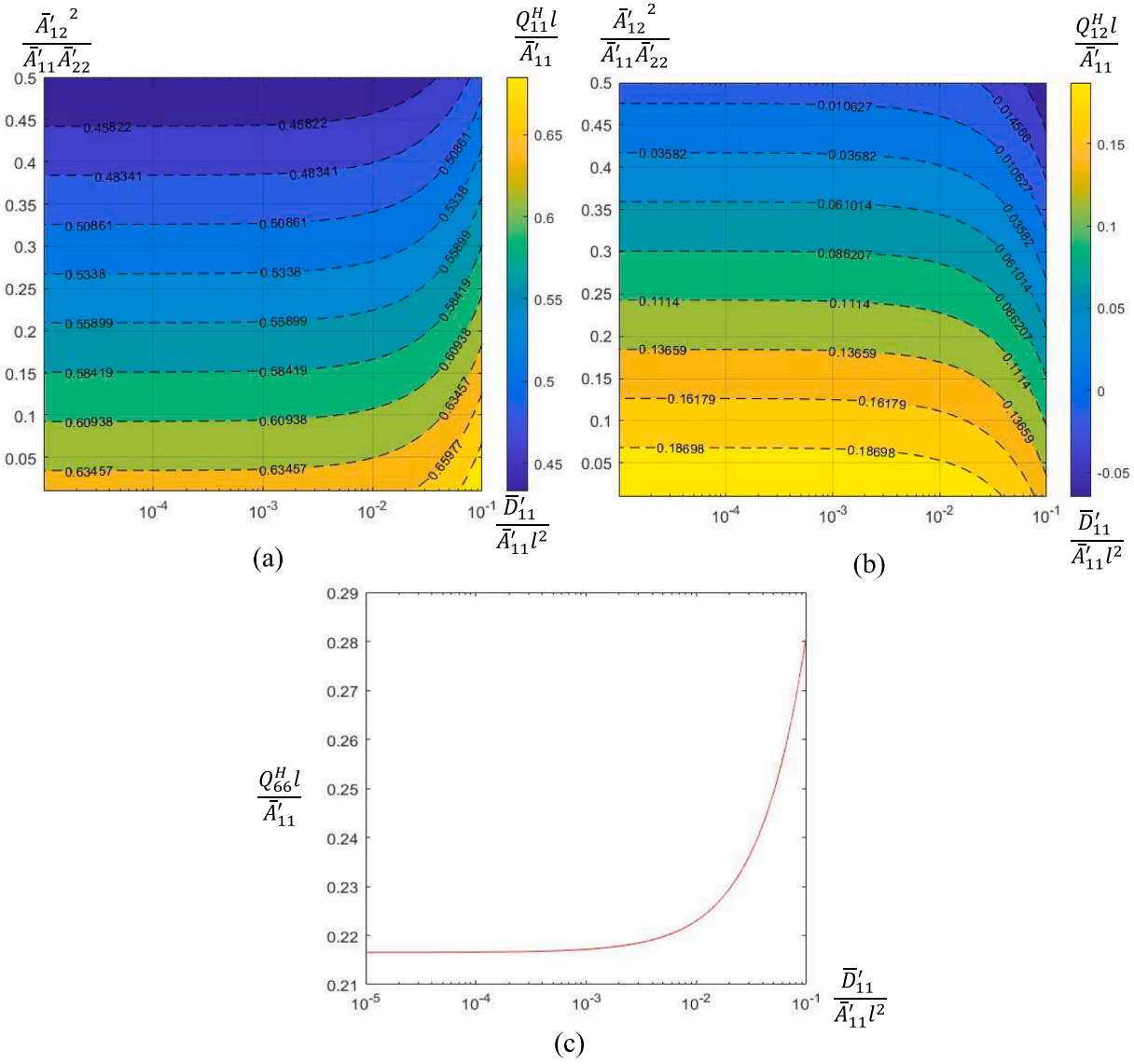

Fig. 20. Influence of wall stiffness parameters on (a) Q_{11}^H or Q_{22}^H (b) Q_{12}^H and (c) Q_{66}^H of triangular core.

Appendix

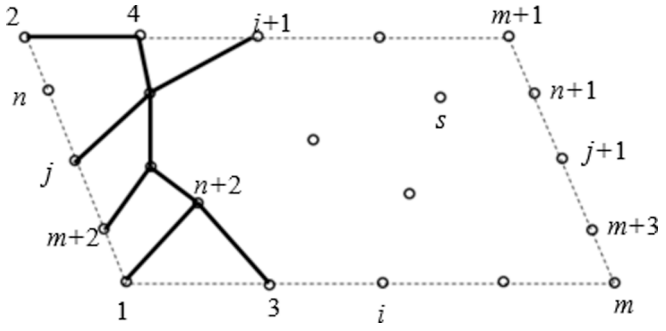

Equations for solving nodal displacements

Applying the periodic boundary conditions to the RVE, we will have the followings;

$\varphi(i) = \varphi(i+1), i = 1, 3, \cdots\ldots, m$

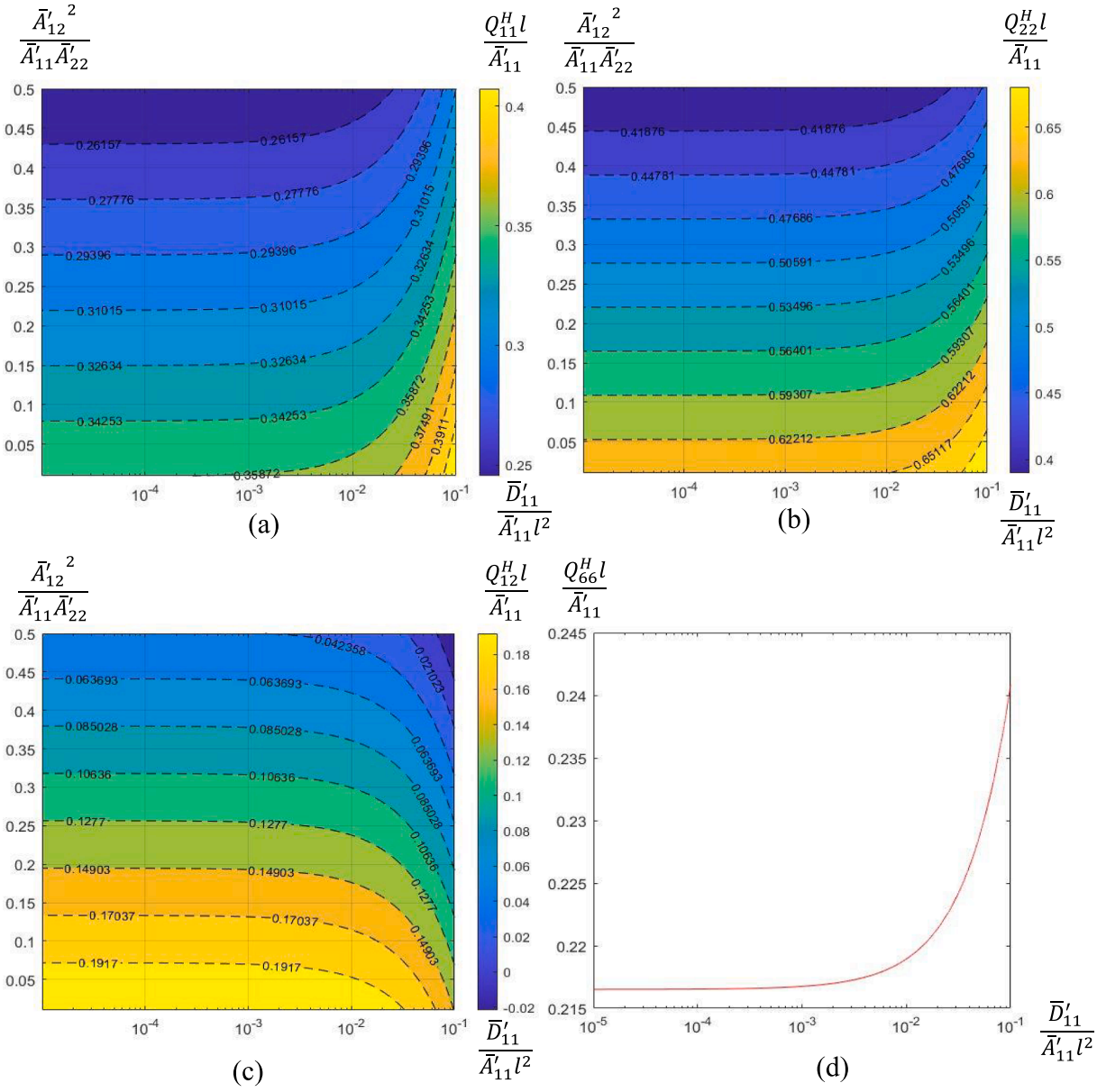

Fig. 21. Influence of wall stiffness parameters on (a) Q_{11}^H (b) Q_{22}^H (c)Q_{12}^H and (d) Q_{66}^H of mixed rhombus-triangular core.

$$u_{(m)l} - u_{(i)l} = u_{(m+1)l} - u_{(i+1)l}, i = 1, 3, \cdots.., m, l = 1, 2, 3$$

$$\varphi(j) = \varphi(j+1), j = (m+2), (m+4), \cdots.., n$$

$$u_{(2)l} - u_{(j)l} = u_{(m+1)l} - u_{(j+1)l}, j = (m+2), (m+4), \cdots.., n, l = 1, 2, 3$$

$$\varphi(1) = \varphi(m). \tag{A.1}$$

RVE does not undergo any rigid body motions, then we will have the followings;

$$u_{(1)1} = 0,\ u_{(1)2} = 0,\ u_{(1)3} = 0, and\ u_{(m)2} = 0. \tag{A.2}$$

Resultant forces at all internal nodes and at all pairs of corresponding nodes i and $i+1$ should be zero, which gives the followings;

$$F_{(1)l} + F_{(2)l} + F_{(m)l} + F_{(m+1)l} = 0, l = 1, 2, 3$$

$$M_{(1)} + M_{(2)} + M_{(m)} + M_{(m+1)} = 0,$$

$$F_{(i)l} + F_{(i+1)l} = 0, i = 3, 5, \cdots.., (m-2) and$$

$$M_{(i)} + M_{(i+1)} = 0, i = (m+2), (m+4), \cdots, n, l = 1, 2, 3$$

$$F_{(k)l} = 0, k = (n+2), (n+3), \cdots, s, l = 1, 2, 3\, M_{(k)l} = 0. \tag{A.3}$$

Equations in (A.1), (A.2) and (A.3) together with the Eqs. (54)-(59) will provide $(4s+3)$ equations to solve for the nodal displacements of RVE. Equations in (A.3) will provide three redundant equations which should be eliminated to solve for the nodal displacements.

References

[1] Tarlochan F, Ramesh S, Harpreet S. Advanced composite sandwich structure design for energy absorption applications: blast protection and crashworthiness. Composites B 2012;43:2198–208.
[2] Manalo A, Aravinthan T. Behavior of full-scale railway turnout sleepers from glue-laminated fiber composite sandwich structures. J Compos Constr 2012;16:724–36.
[3] Crump DA, Dulieu-Barton JM, Savage J. The manufacturing procedure for aerospace secondary sandwich structure panels. J Sandw Struct Mater 2010;12:421–47.
[4] Takeda N, Minakuchi S, Okabe Y. Smart composite sandwich structures for future aerospace application -damage detection and suppression-: a review. J Solid Mech Mater Eng 2007;1:3–17.
[5] Khodaei M, Safarabadi M, Haghighi YM, Farzannia MA. On the ballistic impact behavior of foam-filled honeycomb core/composite skin sandwich panels. J Braz Soc Mech Sci 2023;45:244.
[6] Khodaei M, Safarabadi Farahani M, Haghighi YM. Numerical investigation of high velocity impact on foam-filled honeycomb structures including foam fracture model. Mech Adv Mater Struct 2022;29:748–60.
[7] Fernando D, Teng J, Gattas J, Heitzmann M. Hybrid fibre-reinforced polymer–timber thin-walled structural members. Adv Struct Eng 2018;21:1409–17.
[8] Ou Y, Fernando D, Gattas JM. Experimental investigation of a novel concrete-timber floor panel system with digitally fabricated FRP-timber hollow core component. Constr Build Mater 2019;227:116667.
[9] Ou Y, Gattas JM, Fernando D, Torero JL. Experimental investigation of a timber-concrete floor panel system with a hybrid glass fibre reinforced polymer-timber corrugated core. Eng Struct 2020;203:109832.
[10] Tao Q, Wang C, Wang K, Tan H. Mixed Triangle lattice reinforced membrane antenna reflector: design and analysis. AIAA J 2020;58:1897–900.
[11] Atli-Veltin B, Gandhi F. Effect of cell geometry on the energy absorption of honeycombs under in-plane compression. AIAA J 2010;48:466–78.
[12] Shah UB, Kapania RK. Failure of hexagonal and triangular honeycomb core sandwich panels. AIAA J 2020;58:4923–40.
[13] Montazeri A, Bahmanpour E, Safarabadi M. Three-point bending behavior of foam-filled conventional and auxetic 3D-printed honeycombs. Adv Eng Mater.n/a:2300273.
[14] Safarabadi M, Haghighi YM, Sorkhi M, Yousefi A. Experimental and numerical study of buckling behavior of foam-filled honeycomb core sandwich panels considering viscoelastic effects. J Sandw Struct Mater 2021;23:3985–4015.
[15] Kee Paik J, Thayamballi AK, Sung KG. The strength characteristics of aluminum honeycomb sandwich panels. Thin-Wall Struct 1999;35:205–31.
[16] He W, Yao L, Meng X, Sun G, Xie D, Liu J. Effect of structural parameters on low-velocity impact behavior of aluminum honeycomb sandwich structures with CFRP face sheets. Thin-Wall Struct 2019;137:411–32.
[17] Wang J, Shi C, Yang N, Sun H, Liu Y, Song B. Strength, stiffness, and panel peeling strength of carbon fiber-reinforced composite sandwich structures with aluminum honeycomb cores for vehicle body. Compos Struct 2018;184:1189–96.
[18] Saito K, Pellegrino S, Nojima T. Manufacture of arbitrary cross-section composite honeycomb cores based on origami techniques. J Mech Des 2014;136.
[19] Wei X, Li D, Xiong J. Fabrication and mechanical behaviors of an all-composite sandwich structure with a hexagon honeycomb core based on the tailor-folding approach. Compos Sci Technol 2019;184:107878.
[20] Wei X, Xiong J, Wang J, Xu W. New advances in fiber-reinforced composite honeycomb materials. Sci China Technol Sci 2020;63:1348–70.
[21] Pehlivan L, Baykasoğlu C. An experimental study on the compressive response of CFRP honeycombs with various cell configurations. Composites B 2019;162:653–61.
[22] Sundararaman V, O'Donnell MP, Chenchiah IV, Clancy G, Weaver PM. Stiffness tailoring in sinusoidal lattice structures through passive topology morphing using contact connections. Mater Des 2023;226:111649.
[23] Vitale P, Francucci G, Rapp H, Stocchi A. Manufacturing and compressive response of ultra-lightweight CFRP cores. Compos Struct 2018;194:188–98.
[24] Wei X, Wang Y, Xue P, Zhang T, Rouis A, Xiao W, et al. Carbon fiber composite honeycomb structures and the application for satellite antenna reflector with high precision. Adv Astronaut Sci Technol 2022;5:423–41.
[25] Meddaikar YM, Dillinger JKS, Silva GHC, Breuker RD. Skin panel optimization of the common research model wing using sandwich composites. J Aircr 2022;59:386–99.
[26] Meidell A. Minimum weight design of sandwich beams with honeycomb core of arbitrary density. Composites 2009;40:284–91.
[27] Hudson CW, Carruthers JJ, Robinson AM. Multiple objective optimisation of composite sandwich structures for rail vehicle floor panels. Compos Struct 2010;92:2077–82.
[28] Catapano A, Montemurro M. A multi-scale approach for the optimum design of sandwich plates with honeycomb core. Part II: the optimisation strategy. Compos Struct 2014;118:677–90.
[29] Russell B, Liu T, Fleck N, Deshpande V. Quasi-static three-point bending of carbon fiber sandwich beams with square honeycomb cores. J Appl Mech 2011;78.
[30] Kapania RK, Soliman HE, Vasudeva S, Hughes O, Makhecha DP. Static analysis of sandwich panels with square honeycomb core. AIAA J 2008;46:627–34.
[31] Kreja I. A literature review on computational models for laminated composite and sandwich panels. Cent Eur J Eng 2011;1:59–80.
[32] Somnic J, Jo BW. Status and challenges in homogenization methods for lattice materials. Materials 2022;15.
[33] Gibson LJ, Ashby MF, Schajer GS, Robertson CI. The mechanics of two-dimensional cellular materials. Proc Math Phys Eng Sci 1982;382:25–42.
[34] Masters IG, Evans KE. Models for the elastic deformation of honeycombs. Compos Struct 1996;35:403–22.
[35] Goswami S. On the prediction of effective material properties of cellular hexagonal honeycomb core. J Reinf Plast Compo 2006;25:393–405.
[36] Mukhopadhyay T, Naskar S, Adhikari S. Anisotropy tailoring in geometrically isotropic multi-material lattices. Extreme Mech Lett 2020;40:100934.
[37] Mukherjee S, Adhikari S. A general analytical framework for the mechanics of heterogeneous hexagonal lattices. Thin-Wall Struct 2021;167:108188.
[38] Adhikari S, Mukhopadhyay T, Liu X. Broadband dynamic elastic moduli of honeycomb lattice materials: a generalized analytical approach. Mech Mater 2021;157:103796.
[39] Chen DH, Ozaki S. Analysis of in-plane elastic modulus for a hexagonal honeycomb core: effect of core height and proposed analytical method. Compos Struct 2009;88:17–25.
[40] Chen DH. Equivalent flexural and torsional rigidity of hexagonal honeycomb. Compos Struct 2011;93:1910–7.
[41] Chung J, Waas AM. The inplane orthotropic couple-stress elasticity constants of elliptical cell honeycombs. Int J Eng Sci 2010;48:1123–36.
[42] Gad AI, Gao XL, Li K. A strain energy-based homogenization method for 2-D and 3-D cellular materials using the micropolar elasticity theory. Compos Struct 2021;265:113594.
[43] Li YM, Hoang MP, Abbes B, Abbes F, Guo YQ. Analytical homogenization for stretch and bending of honeycomb sandwich plates with skin and height effects. Compos Struct 2015;120:406–16.
[44] Lin T-C, Chen T-J, Huang J-S. In-plane elastic constants and strengths of circular cell honeycombs. Compos Sci Technol 2012;72:1380–6.
[45] Pan S-D, Wu L-Z, Sun Y-G. Transverse shear modulus and strength of honeycomb cores. Compos Struct 2008;84:369–74.
[46] Malek S, Gibson L. Effective elastic properties of periodic hexagonal honeycombs. Mech Mater 2015;91:226–40.
[47] Hohe J, Becker W. An energetic homogenisation procedure for the elastic properties of general cellular sandwich cores. Composites B 2001;32:185–97.
[48] Hohe J, Becker W. A refined analysis of the effective elasticity tensor for general cellular sandwich cores. Int J Solids Struct 2001;38:3689–717.
[49] Soliman HE, Kapania RK. Equivalent constitutive behavior of sandwich cellular cores. J Sandw Struct Mater 2017;19:424–55.
[50] Grediac M. A finite element study of the transverse shear in honeycomb cores. Int J Solids Struct 1993;30:1777–88.
[51] Catapano A, Montemurro M. A multi-scale approach for the optimum design of sandwich plates with honeycomb core. Part I: homogenisation of core properties. Compos Struct 2014;118:664–76.
[52] Qiu C, Guan Z, Jiang S, Li Z. A method of determining effective elastic properties of honeycomb cores based on equal strain energy. Chin J Aeronaut 2017;30:766–79.
[53] Penado F. Effective elastic properties of honeycomb core with fiber-reinforced composite cells. Open J Compos Mater 2013;03:89–96.
[54] Min L, Fernando D, Gilbert BP, You Z. Hybrid FRP-timber thin-walled Cee section columns under axial compression: Numerical modelling. Thin-Walled Struct 2020;157:107029.
[55] Wang R, Wang J. Modeling of honeycombs with laminated composite cell walls. Compos Struct 2018;184:191–7.
[56] Composites L. In: Mechanics of composite structures. Cambridge: Cambridge University Press; 2003. p. 63–88.
[57] Krishnamurthy T, Saether E. Estimation of effective elastic properties of general multifunctional honeycomb structures using a unit cell method. AIAA Scitech 2019.
[58] Xia Z, Zhang Y, Ellyin F. A unified periodical boundary conditions for representative volume elements of composites and applications. Int J Solids Struct 2003;40:1907–21.
[59] ABAQUS. Software Package, Ver. 2019, Dassault Systemes Simulia Corporation.
[60] Sriharan J. An Inverse approach to the design of cellular core sandwich panels. Edinburgh, UK: Univ. of Edinburgh; 2024. Ph.D. Thesis (submitted).